on Akt and STAT5 resulted from accumulation of Kit(D814Y) at the ER, not from apoptosis. In contrast to Kit(D814Y), in R and pt18 cells, SCF stimulation of Kit(wt) did not activate STAT5 (Fig. 6g), as previously described[27,29]. Accumulation of Kit(wt) on the ER did not affect STAT5 activation (Fig. 6h and Supplementary Fig. 5g), indicating that STAT5 activation requires ER-localized Kit(D814Y). Taken together, these results suggest that newly synthesized partially glycosylated Kit(D814Y) on the ER activates STAT5 aberrantly.

Treatment with monensin or BafA1 for 3 h inhibited Akt independently of apoptosis, and activated STAT5 transiently (Figs 5g and 6i; Supplementary Fig. 5h). These drugs did not enhance STAT5 activity in R cells (Fig. 6j and Supplementary Fig. 5i). These results indicate that accumulated Kit(D814Y) on the Golgi and endosomes can activate STAT5 activation transiently. Thus, mechanisms of negative regulation for STAT5 may exist on the Golgi and endosomes.

The oncogenic role of Kit and its trafficking in rat and human cells. Next, we investigated whether the oncogenic role of Kit(D814Y) and its trafficking seen in RCM cells occur widely in neoplastic mast cells. The human and rat mast cell leukemia cell lines HMC-1 and RBL-2H3 endogenously express Kit with mutations in the kinase domain, these being Kit(D816V) and Kit(D817Y), respectively (Fig. 7a)[12,13]. In these lines, as with RCM, the kinase inhibitor PKC412 blocked Kit kinase activity and cell proliferation (Fig. 7b,c). Most mutant Kit was present as a complex-glycosylated form (Fig. 7d) that significantly co-localized with endolysosomal markers cathepsin D or LAMP1, rather than calnexin (ER) or GM130 (Golgi) (Fig. 7e,f). In HMC-1 cells, anti-Kit staining shows a pattern similar to that of expressed Kit(D814Y)-GFP but not to Kit(wt)-GFP (Supplementary Fig. 6a), confirming the endolysosomal Kit(D816V) staining.

We next examined Kit trafficking to endolysosomes in these cells. Figure 7g shows that PKC412 inhibited trafficking from the PM to endolysosomes, consistent with our findings on Kit(D814Y). Furthermore, for endocytosis, CME inhibition by sucrose reduced the protein levels of Kit but not of p85; in contrast, NCE inhibition by filipin did not affect the protein levels (Fig. 7h and Supplementary Fig. 6b). This suggests that in HMC-1 and RBL-2H3 cells, as in RCM cells, Kit also undergoes CME. Taken together, these results suggest that, in HMC-1 and RBL-2H3, Kit's oncogenic role and intracellular trafficking are similar to those in RCM cells.

Kit signalling occurs in distinct compartments in human and rat cells. Next, we examined the subcellular location for signalling in HMC-1 and RBL-2H3. As in RCM, oncogenic activation of Akt and STAT5 was also seen and was prevented by PKC412 (Fig. 8a and Supplementary Fig. 6c). Blockade of Kit trafficking to endolysosomes by BafA1 for 24 h also suppressed the activation of Akt but not of STAT5 (Fig. 8b and Supplementary Fig. 6d), indicating that endolysosomal localization of Kit is essential for Akt activation. Blockade of ER export of Kit by BFA for 16 h suppressed Akt activation, but enhanced STAT5 activation (Fig. 8c). Collectively, these results suggest that in HMC-1 and RBL-2H3 cells, as in RCM cells, partially glycosylated Kit aberrantly activates STAT5 on the ER.

Discussion

In contrast to normal Kit, which signals from the PM, mutant oncogenic Kit signals from intracellular compartments (Fig. 8d). Newly synthesized, incompletely glycosylated mutant Kit initially localizes to the ER then activates STAT5. Subsequently, mutant Kit traffics to the PM through the Golgi along the secretory pathway and then immediately undergoes CME due to its kinase activity. It then accumulates in endolysosomes, but is not fully ubiquitinated. Mutant Kit is constitutively associated with PI3K, but the complex activates Akt only on the cytoplasmic surface of endolysosomes. In addition to previous reports[25,26,30–33], our study shows that the oncogenic signalling from mutant Kit is spatially distinct from normal signalling. By comparing RCM with R cells, we believe that our results show the significance of the unusual Kit localization seen in neoplastic mast cells.

Compartment-dependent oncogenic signalling by constitutively active growth factor receptors has occasionally been reported before. In multiple myeloma cells, deregulated FGF receptor 3 mutants accumulate at the Golgi, and initiate Erk1/2 and STAT1/3 signalling[22,27]. Oncogenic gp130 activates STAT3 not only on the ER but also on endosomes in hepatocytes[59]. In acute myeloid leukemia, the oncogenic Flt3 mutant Flt3-ITD activates STAT5 only on the ER[25–27], as shown here for mutant Kit. Kit(D816V) directly tyrosine-phosphorylates STAT proteins *in vitro*[21], suggesting that STAT5 might act as a substrate for ER-localized mutant Kit. The Kit-STAT5 complex might escape from negative regulators such as protein tyrosine phosphatases on the ER but not on the Golgi, endosomes or the PM. The signalling platform may depend on the receptor and type of cell. These studies support our model that oncogenic Kit signalling occurs only on specific intracellular compartments in neoplastic mast cells. In leukaemia, mutant Kit participates in the PI3K-Akt pathway, in STAT5 activation, in the RhoA-Rho kinase pathway[47] and in activation of Src-like adaptor protein[60], and there is great interest in further understanding the spatial organization of this signalling.

Mutant Kit associates with PI3K throughout its intracellular trafficking, but only activates Akt when on endolysosomes. The PI3K product $PI(3,4,5)P_3$, which is required for Akt activation, is

Figure 6 | Kit(D814Y) at the ER activates STAT5 in mouse cells. (**a**,**b**) Inhibition of export of Kit(D814Y) from the Golgi. RCM cells were cultured with 250 nM monensin (inhibits Golgi transport) for 24 h. (**a**) RCM cells were stained with anti-Kit (green) and anti-GM130 (Golgi marker, blue). Magnified images of the boxed area are shown. Bars, 10 μm. The graph shows correlation coefficient (Pearson's R) between Kit and GM130. Results are means ± s.d. from 15 cells. ***$P<0.001$, Student's *t*-test. (**b**) Immunoblots of anti-Kit immuoprecipitates (left) and cell lysates (right). (**c**–**e**) Inhibition of export of Kit(D814Y) from the ER. RCM cells were cultured with 1 μg ml^{-1} tunicamycin for 24 h, or 5 μM BFA for 16 h to block ER export. (**c**) RCM cells were stained with anti-Kit (green) and anti-calnexin (ER marker; red). Magnified images of the boxed area are shown. Bars, 10 μm. The graph shows the correlation coefficient (Pearson's R) between Kit and calnexin. Results are means ± s.d. from 11 to 13 cells. Data were subjected to one-way ANOVA with Dunnett's multiple comparison *post-hoc* test. ***$P<0.001$. (**d**) Immunoblots of anti-Kit immuoprecipitates and cell lysates. NB: ER-localized Kit(D814Y) activated STAT5. (**e**) BFA-treated cells were stained with anti-Kit (green) and anti-STAT5 (red) antibodies. Magnified images of the boxed area are shown. Bars, 10 μm. The graph shows the correlation coefficient (Pearson's R) between Kit and STAT5 in the non-nuclear region. Results are means ± s.d. from 16 cells. ***$P<0.001$, Student's *t*-test. NB: accumulation of Kit(D814Y) in the ER significantly enhanced co-localization with STAT5. (**f**) RCM cells were treated with 5 μM BFA, 1 μg ml^{-1} tunicamycin, 250 nM monensin or 100 nM BafA1 for the indicated periods and then immunoblotted. (**g**) Starved R cells (left) or pt18 cells (right) stimulated with 50 ng ml^{-1} SCF for 5 min then lysed and immunoblotted. NB: normal Kit was unable to activate STAT5. (**h**–**j**) RCM cells or starved R cells treated with 250 nM monensin or 5 μM BFA for the indicated periods, then immunoblotted. CG = complex-glycosylated form; DG = deglycosylated form; HM = high mannose form.

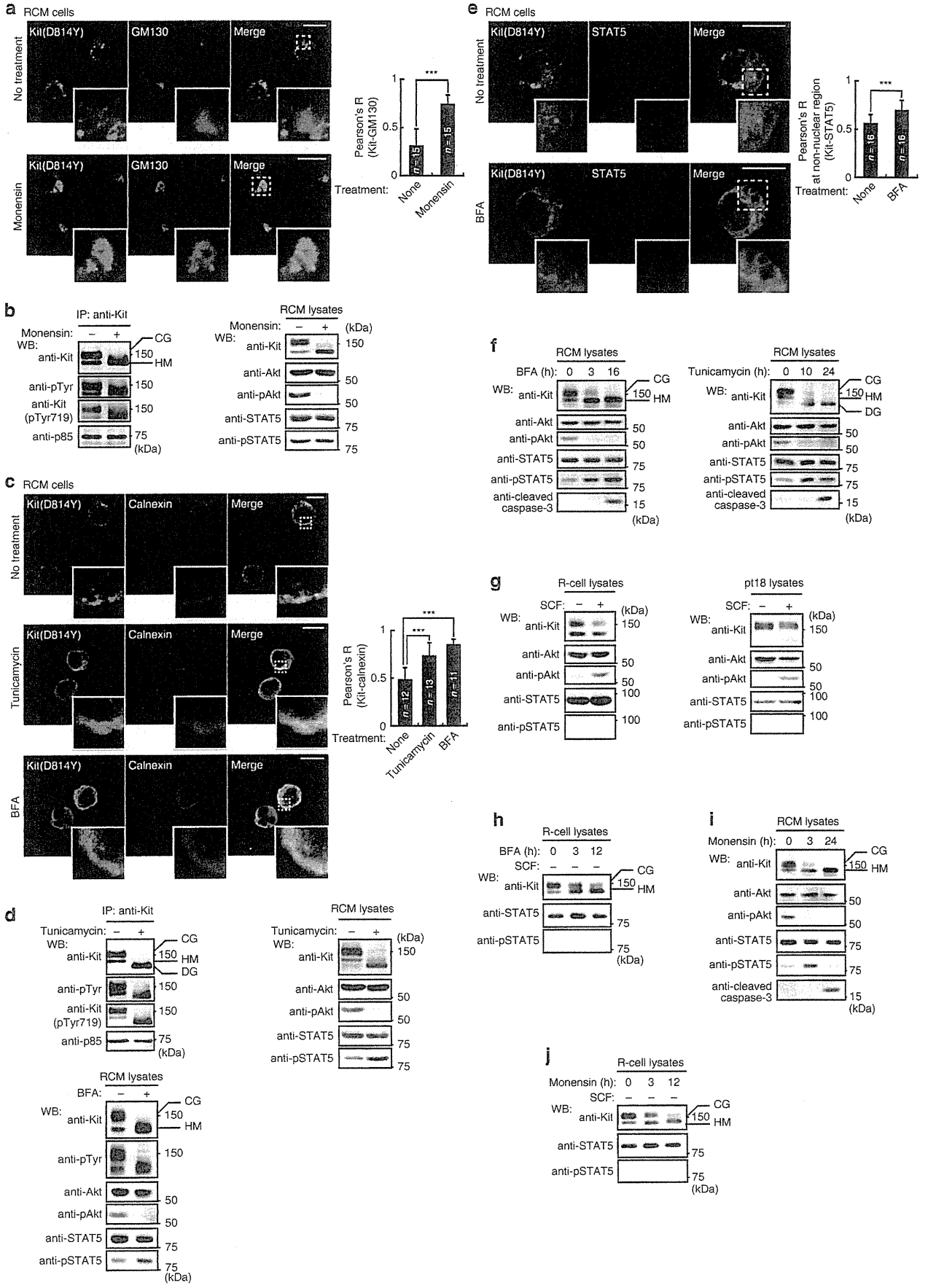

believed to be generated solely at the PM[54,61,62]. However, $PI(4,5)P_2$, a substrate of PI3K, is generated by phosphatidylinositide-4-phosphate-5-kinase on LAMP1-positive structures for proto-lysosome homeostasis[63,64] and plays a role in endosome-to-lysosome trafficking[52]. The following observation is also relevant: when SCF binds Kit at the PM, Kit activates inositol-5-phosphatase, which dephosphorylates $PI(3,4,5)P_3$, and so terminates Akt signalling[10]. The significance is that, unlike normal Kit, mutant Kit cannot activate Akt at the PM. Further studies will be required to understand the mechanism by which the Kit-PI3K complex activates Akt selectively on endolysosomes.

In this study, CME stabilized mutant Kit on endolysosomes. This agrees with previous data showing that CME is essential for sustained signalling from Met, TGFβR and EGFR[24,37–39,50]. However, mutant Kit was barely found in recycling endosomes, where the other receptors localize after ligand stimulation, and then recycle back to the PM. As very little SCF-bound normal Kit and mutant Kit recycle back to the PM[33,45], CME must lead to at least two different pathways: the endolysosomal pathway leading to receptor destruction and the recycling endosome pathway, leading to receptor recycling. Ubiquitination of mutant Kit is insufficient for its rapid degradation. Defects in the tumour suppressor protein Cbl, an E3-ubiquitin ligase, also slow the degradation of Kit and Flt3, and prolong the activation of Akt, resulting in mastocytosis and myelo-proliferative disease[43,65,66]. When the CME pathway was blocked, mutant Kit was sorted into NCE and normally ubiquitinated. Neoplastic transformation might also involve an inappropriate sorting mechanism that recruits mutant Kit predominantly into CME not NCE. At present, we cannot explain why.

After SCF stimulation, Kit(wt) is transported into lysosomes in a manner dependent on ESCRT. This is consistent with previous reports that ESCRT transports ubiquitinated cargos[44,46,52]. ESCRT inhibition, however, does not cause accumulation of Kit(D814Y). Importantly, a recent study described that under-ubiquitinated cargos are incorporated into lysosomes in a manner independent of ESCRT[46]. Our results suggest that the mechanism of endosome-lysosome trafficking for mutant Kit is different from that for Kit(wt). Other mutant RTKs, such as EGFR(L858R)[23], Met(D1246N)[24] and Flt3(D835Y)[25], might also escape from ESCRT-dependent trafficking.

Imatinib, a Kit inhibitor used as a drug, is efficacious in most patients with gastrointestinal stromal tumours harbouring Kit mutations in the juxta-membrane region[4,11,14]. However, imatinib is ineffective for most human mast cell tumours with Kit mutations in the kinase domain[20,29,67]. Moreover, during imatinib treatment of the gastrointestinal tumours, mutations often develop in the Kit kinase domain[14]. Imatinib-resistant gastrointestinal tumour cells depend on activation of the PI3K-Akt pathway by Kit mutants for their proliferation, and so resemble mast cells[68].

In this study, we showed that, in mast cells, mutant Kit trafficking to endolysosomes is critical for the activation of Akt. When acute myeloid leukemia cells with constitutively active Flt3 mutants, such as Flt3-ITD and Flt3(D835Y), are treated with statins (HMG-CoA reductase inhibitors), this reduces Akt activation by blocking receptor trafficking towards the PM[25]. Thus, Kit trafficking could be a new therapeutic target for mast cell tumours, and for imatinib-resistant gastrointestinal tumours. Combined therapy with an antibody and a kinase inhibitor seems attractive. As PKC412 treatment causes mutant Kit to remain at the PM through blocking the Kit kinase activity, it might enhance the activity of anti-Kit antibody[69]. Lapatinib, an EGFR kinase inhibitor, enhances the cytotoxic activity of trastuzumab, an anti-ErbB2 antibody *in vivo*[70].

In conclusion, we show that compartment-dependent oncogenic Kit signalling is necessary for neoplastic mast cell proliferation. These findings provide new insights into the pathogenic role of Kit in neoplastic mast cell disorders. Improper trafficking and aberrant signalling are frequent features of constitutively active growth factor receptors, for which these data will shed light on the significance of the spatial organization of this oncogenic signalling.

Methods

Cells and stimulation. RCM (R cell, mutant Kit) and R cells were established from splenocytes of DO11.10 mice by repeated stimulation with ovalbumin peptides *in vitro*. The cell lines exhibited mast cell-like surface phenotype, c-Kit$^+$ FcεRI$^+$, and mast cell-like expression profiles of proteases. Moreover, RCM and R cells can secrete biologically active product on stimulation *in vitro* and *in vivo*. They do not express SCF. We were unable to find *Kit(wt)* by cDNA sequencing in RCM cells. For culture of R cells, we used culture supernatants from T-cell lines stimulated with an anti-T cell receptor antibody as a cytokine cocktail. R cells were cultured in 0.25% cytokine cocktail. RCM cells proliferated without the cocktail and developed tumours *in vivo*. HMC-1.2 (referred to henceforth as HMC-1), RBL-2H3 and pt18 cells were fro m Dr Hirohisa Saito and Dr Kenji Matsumoto (National Center for Child Health and Development), Dr Ko Okumura (Juntendo University) and Dr Ryo Goitsuka (Tokyo University of Science), respectively. These cells and RCM cells were cultured at 37 °C in RPMI1640 medium supplemented with 10% fetal calf serum (FCS), penicillin, streptomycin and 50 μM 2-mercaptoethanol. HMC-1 cells were grown in suspension at 37 °C in α-MEM containing 10% FCS, penicillin and streptomycin. For stimulation, cells were starved for at least 3 h and then treated with 50 ng ml^{-1} recombinant mouse SCF (PeproTech).

Cell proliferation assay. Cells were cultured with inhibitors or cytokines for at least 16 h and then treated with [^{3}H]-thymidine deoxyribonucleotide (TdR) for 8 h. Cell proliferation was evaluated by incorporation of [^{3}H]-TdR.

Chemicals. PKC412 (Santa Cruz Biotechnology), cytochalasin D (Sigma-Aldrich), tunicamycin (Sigma-Aldrich), cycloheximide (Sigma-Aldrich), filipin (Sigma-Aldrich), Akt inhibitor VIII (Calbiochem), STAT5 inhibitor (Calbiochem), LY294002 (Calbiochem), U0126 (Calbiochem) and pitstop2 (Abcam) were dissolved in dimethyl sulfoxide. Bafilomycin A1 (Sigma-Aldrich), brefeldin A (Sigma-Aldrich) and monensin (Biomol) were dissolved in ethanol.

Figure 7 | Oncogenic role and intracellular trafficking of mutant Kit in rat and human cells. (**a**) Mutant Kit is constitutively active in HMC-1 and RBL-2H3 cells. (Left) Schematic structures of Kit in HMC-1 and RBL-2H3 cells. (Right) Immunoblots of anti-Kit immunoprecipitates from HMC-1 or RBL-2H3 cells treated with 1 μM PKC412 (Kit kinase inhibitor) for 4 or 12 h, respectively. (**b**,**c**) The effect of PKC412 on proliferation. (**b**) [^{3}H]-thymidine incorporation in HMC-1 cells treated with PKC412 for 24 h. Results (c.p.m.) are means ± s.d. ($n=3$). (**c**) Growth of RBL-2H3 cells treated with (filled circles) or without (open circles) 1 μM PKC412. Results are means ± s.d. ($n=3$). (**d**) Glycosylation of Kit(D816V) and Kit(D817Y) performed as for Fig. 2a. (**e**,**f**) Subcellular localization of Kit. (**e**) Methanol-fixed HMC-1 or (**f**) PFA-fixed RBL-2H3 cells were double-stained with anti-Kit (green) and anti-cathepsin D (endolysosome marker; red), anti-LAMP1 (endolysosome marker; red), anti-calnexin (ER marker; red), or anti-GM130 (Golgi marker; blue). Magnified images of the boxed area are shown. Representative images of Kit-positive endolysosomes containing cathepsin D are shown. Bars, 5 μm. The graphs show the correlation coefficient (Pearson's R) between Kit and organelle markers. Results are means ± s.d. from 15 to 18 cells. Data were subjected to one-way ANOVA with Dunnett's multiple comparison *post-hoc* test. $^{**}P<0.01$, $^{***}P<0.001$. (**g**,**h**) Endocytosis of mutant Kit in HMC-1 and RBL-2H3 cells. (**g**) HMC-1 (left) or RBL-2H3 cells (right) treated with 1 μM PKC412 for 4 or 12 h, respectively. Cells were stained with anti-Kit (green) and anti-calnexin (ER marker; red). Insets show boxed areas at higher magnification. Bars, 10 μm. (**h**) HMC-1 cells treated with 1 μg ml^{-1} filipin or 0.45 M sucrose for 3 h to block endocytosis. Cells were stained with anti-Kit (cyan) and anti-p85 (red). Bars, 10 μm. Immunoblots for Kit, p85 and TfR are shown.

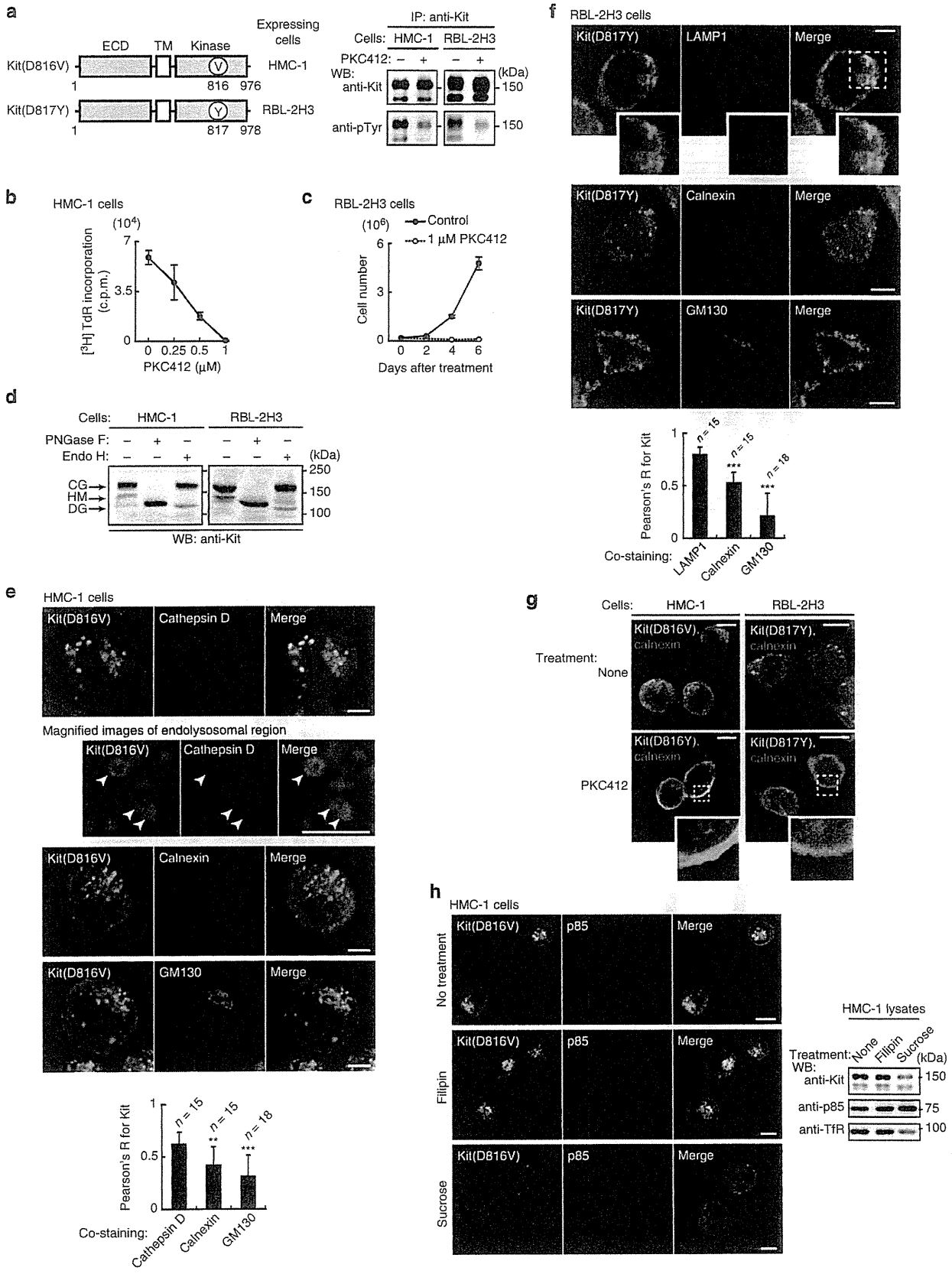

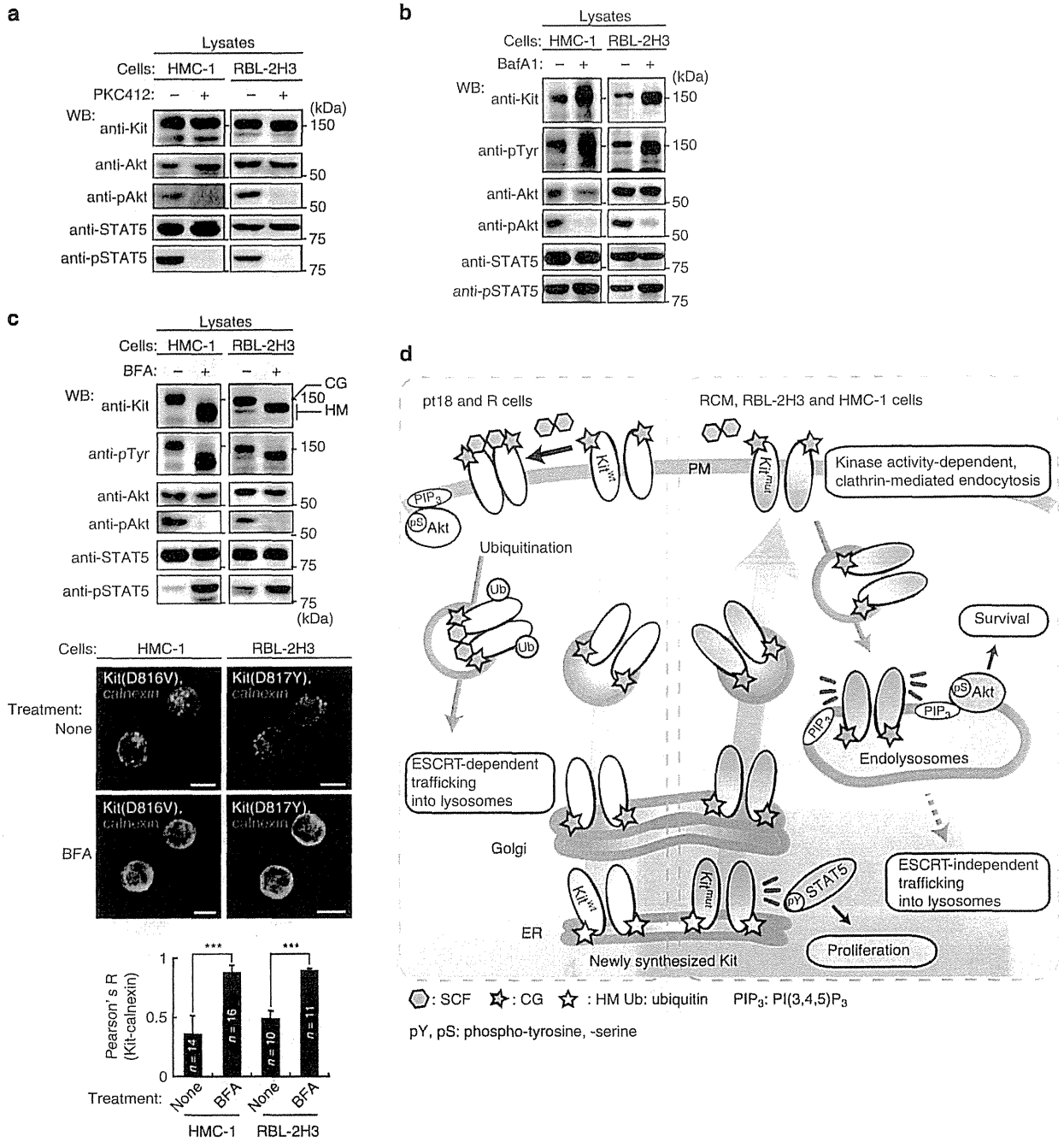

Figure 8 | Oncogenic signalling by mutant Kit on endolysosomes and the ER in rat and human cells. (**a**) Constitutive activation of Akt and STAT5 by mutant Kit in HMC-1 and RBL-2H3 cells. Immunoblots, HMC-1 (left) or RBL-2H3 cells (right) treated with 1 μM PKC412 for 4 or 12 h, respectively. (**b**) Immunoblots, HMC-1 or RBL-2H3 cells cultured with 100 nM BafA1 for 24 h. (**c**) (Top) Immunoblots, HMC-1 or RBL-2H3 cells cultured with 5 μM BFA for 16 h. CG, complex-glycosylated form; HM, high mannose form. (Middle) Cells stained with anti-Kit(green) and anti-calnexin (ER marker; red). Bars, 10 μm. (Bottom) The graph shows the correlation coefficient (Pearson's R) between Kit and calnexin. Results are means ± s.d. from 10 to 16 cells. ***$P < 0.001$, Student's *t*-test. (**d**) Trafficking and signalling from normal Kit (left) and mutant Kit (right). Normal Kit-left panel; newly synthesized Kit traffics from ER, through the Golgi apparatus to the PM. After binding to SCF, Kit activates downstream pathways such as PI3K-Akt mainly at the PM. Kit then becomes endocytosed and ubiquitinated, resulting in ESCRT-dependent incorporation into lysosomes and rapid degradation. Mutant Kit-right panel; soon after synthesis, immature Kit is localized on the ER and activates STAT5. It then traffics to the PM along the secretory pathway, similar to normal Kit. After mutant Kit reaches the PM, it immediately undergoes clathrin-mediated endocytosis in a kinase activity-dependent manner. Kit then accumulates to endolysosomes but is not fully ubiquitinated, so is resistant to degradation. Unlike normal Kit, mutant Kit-PI3K activates Akt specifically on endolysosomes. Mutant Kit does not require ESCRT for incorporation into lysosomes.

Antibodies. The following antibodies were purchased: c-Kit (M-14), STAT3 (C-20), STAT5 (C-17), Erk2 (K-23), Jak2 (C-20), cathepsin D (H-75), CD63 (H-93), actin (I-19) and CD28 (H-193) from Santa Cruz Biotechnology; Kit[pTyr719], Akt, Akt[pSer473], STAT5[pTyr694] (D47E7), cleaved caspase-3 and Erk[pThr202/pTyr204] (E10) from Cell Signaling Technology; TGN46, EEA1, Rab11, Tsg101 and TfR from Abcam; calnexin and ubiquitin (FK2) from Enzo; GM130 (35) and AP2α (8) from BD Transduction Laboratories; p85 from Millipore and LAMP1 from Sigma-Aldrich. Anti-phosphotyrosine antibody (4G10) was kindly provided by Dr Toshinori Nakayama (Chiba University). Alexa-fluor 488 anti-Kit (AF488-anti-Kit; 2B8; Biolegend) was used for the experiments in Figs 2b and 5k. The list of antibodies with source and conditions of immunoblotting and immunofluorescence is shown in Supplementary Table 1. HRP-labelled anti-mouse Ig, anti-rabbit Ig and anti-goat Ig secondary antibodies were purchased from The Jackson Laboratory. AF488-anti-goat IgG, AF568-anti-rabbit IgG, AF647-anti-goat IgG and AF647-anti-mouse secondary antibodies were obtained from Molecular Probes.

Plasmids. Mouse cDNAs encoding Kit(wt) or Kit(D814Y) were generated by reverse transcription polymerase chain reaction from R or RCM cells, respectively. After deletion of the termination codon, they were fused with GFP from pEGFP-N1 (Clontech). For protein expression, constructs were subcloned into the Xho I and Not I sites of pBCMGS (from Dr Hajime Karasuyama, Tokyo Medical and Dental University). PH-GFP or PH(R25C)-GFP subcloned into pEGFP-N1 (ref. 54) were from Dr Tamás Balla (National Institutes of Health) through Addgene. The human p85 N-terminal SH2 domain (325–430) or C-terminal SH2 domain (614–721) subcloned into pGEX-4T-2 (GE Healthcare Life Sciences) were from Dr Masayuki Oda (Kyoto Prefectural University).

Gene silencing with siRNAs. For silencing *Kit(D814Y)*, *STAT5B*, *AP2α* or *Tsg101*, siRNA duplexes were purchased from Sigma-Aldrich (Kit1: 5′-GAAGGAUUAUGUCAAAUCUTT-3′, Kit2: 5′-GACAUGAAGCCUGGCGUUUTT-3′, STAT5-1: 5′-GAAUUUGCCAGGACGGAAUTT-3′, STAT5-2: 5′-GGAAUUACACUUUCUGGCATT-3′, Tsg1: 5′-GACACATACCCATATAACCCC-3′, Tsg2: 5′-ACCCGCTTAGATCAAGAAGTA-3′, AP2α-1: 5′-GCAAAGAGGCTGAGATCAAGA-3′, AP2α-2: 5′-GGGTTATGCTGCCAAGACAGT-3′). The control siRNA duplex was purchased from Sigma-Aldrich (Mission negative control SIC-001). No STAT5A was observed in RCM cells.

Transfection. For protein expression or knockdown, cells were transfected by using a Gene Pulser II electroporation system (Bio-Rad Laboratory) and cultured for at least 20 h. Cells expressing Kit(D814Y)-GFP, PH-GFP or PH(R25C)-GFP were selected in 1 mg ml^{-1} G-418.

Immunofluorescence. Cells were fixed with 4% PFA for 20 min at room temperature, or with methanol for 10 min at −20 °C, then cyto-centrifuged onto coverslips. Fixed cells were permeabilized and blocked for 30 min in PBS supplemented with 0.1% saponin and 3% bovine serum albumin, and then incubated with a primary and a secondary antibody for 1 h each. To stain with anti-Akt(pSer473) (Cell Signaling Technology; 193H12), 10% skimmed milk was used for blocking. After washing with PBS, cells were mounted with Fluomount (DiagnosticBioSystems). For staining endocytic compartments, cells were incubated for 1 h with 5 μg ml^{-1} AF647-CTXB or 1 mg ml^{-1} AF647-dextran (Molecular Probes). Confocal images were obtained by a Fluoview FV10i laser scanning microscope with an x60 1.20 N.A. water-immersion objective (Olympus). Composite figures were prepared with Photoshop elements 10 and Illustrator CS6 software (Adobe). Pearson's correlation coefficients (Pearson's R) were calculated with NIH ImageJ Version 1.48v software.

Immunoprecipitation and western blotting. Lysates from RCM, R, pt18, HMC-1 or RBL-2H3 cells were prepared in NP-40 lysis buffer (50 mM HEPES, pH 7.4, 10% glycerol, 1% NP-40, 4 mM EDTA, 100 mM NaF, 1 μg ml^{-1} aprotinin, 1 μg ml^{-1} leupeptin, 1 μg ml^{-1} pepstatin A, 1 mM PMSF and 1 mM Na_3VO_4). Kit from 2×10^6 cells was immunoprecipitated in each assay. Immunoprecipitation was performed at 4 °C for 5 h using protein-G pre-coated with 1 μg of antibody. Samples were dissolved in SDS–polyacrylamide gel electrophoresis (SDS–PAGE) sample buffer, and subjected to SDS–PAGE and electro-transferred onto PVDF membranes. Immunodetection was performed by ECL (PerkinElmer). Sequential re-probing of membranes was performed after the complete removal of primary and secondary antibodies in stripping buffer (Thermo Scientific), or inactivation of peroxidase by 0.1% NaN_3. Results were analysed with an LAS-3000 image analyzer with Science Lab software (Fujifilm Co.) or with a c-Digit imaging system with Image Studio Digit software (Licor Biosciences). Uncropped versions of the most important blots are shown in Supplementary Figs 7–11.

Purification of endolysosomal vesicles. Homogenates from RCM or R cells were prepared by re-suspending in hypotonic buffer (20 mM HEPES pH 7.4, 1 mM $MgCl_2$, 4 mM NaF, 10 mM EDTA, 0.01% NP-40, 1 μg ml^{-1} aprotinin, 1 μg ml^{-1} leupeptin, 1 μg ml^{-1} pepstatin A, 1 mM PMSF and 1 mM Na_3VO_4), and subsequent Dounce homogenization (20 strokes). The suspension was pre-cleared by centrifuging at 1,000 × *g* for 10 min at 4 °C. Endolysosomes were immunoprecipitated with anti-LAMP1-coated protein-G Dynabeads (Veritas) and subjected to immunoblotting. Rabbit anti-CD28 antibody was used for control IgG. Immunoprecipitation was performed at 4 °C for 12 h using 1.5 μg of anti-LAMP1 or anti-CD28. For each assay, 5×10^6 cells were used.

GST-pulldown assay. GST-fusion proteins were expressed in the *E. coli* BL-21 strain on incubation with 0.5 mM IPTG at 22 °C for 12 h. The bacteria were lysed by sonication in RIPA buffer (50 mM HEPES, pH 7.4, 10% glycerol, 0.1% SDS, 0.25% sodium deoxycholate, 1% NP-40, 4 mM EDTA, 100 mM NaF, 1 μg ml^{-1} aprotinin, 1 μg ml^{-1} leupeptin, 1 μg ml^{-1} pepstatin A, 1 mM PMSF). GST-fusion proteins were collected on glutathione-Sepharose beads from RIPA lysates and washed four times with RIPA buffer. Pull-down assays were performed at 4 °C for 5 h in NP-40 lysates prepared from RCM or R cells. Kit from 1×10^6 cells was pulled down in each assay. After extensively washing with NP-40 lysis buffer, the bead pellets were analysed by SDS–PAGE and immunoblotted with an anti-Kit antibody.

Analysis of protein glycosylation. Following the manufacturer's instructions (New England Biolabs), NP-40 cell lysates were treated with endoglycosidase H or peptide-N-glycosidase F for 1 h at 37 °C. The reactions were stopped with SDS–PAGE sample buffer, products were resolved by SDS–PAGE and immunoblotted with an anti-Kit antibody.

References

1. Besmer, P. *et al.* A new acute transforming feline retrovirus and relationship of its oncogene v-kit with the protein kinase gene family. *Nature* **320,** 415–421 (1986).
2. Yarden, Y. *et al.* Human proto-oncogene c-kit: a new cell surface receptor tyrosine kinase for an unidentified ligand. *EMBO J.* **6,** 3341–3351 (1987).
3. Blume-Jensen, P. & Hunter, T. Oncogenic kinase signalling. *Nature* **411,** 355–365 (2001).
4. Kitamura, Y. & Hirota, S. Kit as a human oncogenic tyrosine kinase. *Cell Mol. Life Sci.* **61,** 2924–2931 (2004).
5. Rönnstrand, L. Signal transduction via the stem cell factor receptor/c-Kit. *Cell Mol. Life Sci.* **61,** 2535–2548 (2004).
6. Roskoski, R. Structure and regulation of Kit protein-tyrosine kinase—the stem cell factor receptor. *Biochem. Biophys. Res. Commun.* **338,** 1307–1315 (2005).
7. Blume-Jensen, P., Janknecht, R. & Hunter, T. The kit receptor promotes cell survival via activation of PI 3-kinase and subsequent Akt-mediated phosphorylation of Bad on Ser136. *Curr. Biol.* **8,** 779–782 (1998).
8. Timokhina, I., Kissel, H., Stella, G. & Besmer, P. Kit signaling through PI 3-kinase and Src kinase pathways: an essential role for Rac1 and JNK activation in mast cell proliferation. *EMBO J.* **17,** 6250–6262 (1998).
9. Broudy *et al.* Signaling via Src family kinases is required for normal internalization of the receptor c-Kit. *Blood* **94,** 1979–1986 (1999).
10. Ma, P. *et al.* Balanced interactions between Lyn, the p85α regulatory subunit of class IA phosphatidylinositol-3-kinase, and SHIP are essential for mast cell growth and maturation. *Mol. Cell Biol.* **31,** 4052–4062 (2011).
11. Hirota, S. *et al.* Gain-of-function mutations of c-kit in human gastrointestinal stromal tumors. *Science* **279,** 577–580 (1998).
12. Furitsu, T. *et al.* Identification of mutations in the coding sequence of the proto-oncogene c-kit in a human mast cell leukemia cell line causing ligand-independent activation of c-kit product. *J. Clin. Invest.* **92,** 1736–1744 (1993).
13. Boissan, M., Feger, F., Guillosson, J. J. & Arock, M. c-Kit and c-kit mutations in mastocytosis and other hematological diseases. *J. Leukoc. Biol.* **67,** 135–148 (2000).
14. Lasota, J. & Miettinen, M. Clinical significance of oncogenic KIT and PDGFRA mutations in gastrointestinal stromal tumours. *Histopathology* **53,** 245–266 (2008).
15. Chian, R. *et al.* Phosphatidylinositol 3 kinase contributes to the transformation of hematopoietic cells by the D816V c-Kit mutant. *Blood* **98,** 1365–1373 (2001).
16. Aichberger, K. J. *et al.* Identification of proapoptotic Bim as a tumor suppressor in neoplastic mast cells: role of KIT D816V and effects of various targeted drugs. *Blood* **114,** 5342–5351 (2009).
17. Jahn, T., Leifheit, E., Gooch, S., Sindhu, S. & Weinberg, K. Lipid rafts are required for Kit survival and proliferation signals. *Blood* **110,** 1739–1747 (2007).
18. Gordon, P. M. & Fisher, D. E. Role for the proapoptotic factor BIM in mediating imatinib-induced apoptosis in a c-KIT-dependent gastrointestinal stromal tumor cell line. *J. Biol. Chem.* **285,** 14109–14114 (2010).
19. Ning, Z. Q., Li, J. & Arceci, R. J. Signal transducer and activator of transcription 3 activation is required for Asp816 mutant c-Kit-mediated cytokine-independent survival and proliferation in human leukemia cells. *Blood* **97,** 3559–3567 (2001).

20. Baumgartner, C. *et al.* Expression of activated STAT5 in neoplastic mast cells in systemic mastocytosis: subcellular distribution and role of the transforming oncoprotein KIT D816V. *Am. J. Pathol.* **175,** 2416–2429 (2009).
21. Chaix, A. *et al.* Mechanisms of STAT protein activation by oncogenic KIT mutants in neoplastic mast cells. *J. Biol. Chem.* **286,** 5956–5966 (2009).
22. Ronchetti, D. *et al.* Deregulated FGFR3 mutants in multiple myeloma cell lines with t(4;14): comparative analysis of Y373C, K650E and the novel G384D mutations. *Oncogene* **20,** 3553–3562 (2003).
23. Chung, B. M. *et al.* Aberrant trafficking of NSCLC-associated EGFR mutants through the endocytic recycling pathway promotes interaction with Src. *BMC. Cell Biol.* **10,** 84 (2009).
24. Joffre, C. *et al.* A direct role for Met endocytosis in tumorigenesis. *Nat. Cell Biol.* **13,** 827–837 (2011).
25. Williams, A. B. *et al.* Fluvastatin inhibits FLT3 glycosylation in human and murine cells and prolongs survival of mice with FLT3/ITD leukemia. *Blood* **120,** 3069–3079 (2012).
26. Choudhary, C. *et al.* Mislocalized activation of oncogenic RTKs switches downstream signaling outcomes. *Mol. Cell* **36,** 326–339 (2009).
27. Toffalini, F. & Demoulin, J. B. New insights into the mechanisms of hematopoietic cell transformation by activated receptor tyrosine kinases. *Blood* **116,** 2429–2437 (2010).
28. Mitsui, H. *et al.* Development of human mast cells from umbilical cord blood cells by recombinant human and murine c-kit ligand. *Proc. Natl Acad. Sci. USA* **90,** 735–739 (1993).
29. Growney, J. D. *et al.* Activation mutations of human c-KIT resistant to imatinib mesylate are sensitive to the tyrosine kinase inhibitor PKC412. *Blood* **106,** 721–724 (2005).
30. Xiang, Z., Kreisel, F., Cain, J., Colson, A. L. & Tomasson, M. H. Neoplasia driven by mutant c-KIT is mediated by intracellular, not plasma membrane, receptor signaling. *Mol. Cell Biol.* **27,** 267–282 (2007).
31. Tabone-Eglinger, S. *et al.* KIT mutations induce intracellular retention and activation of an immature form of the KIT protein in gastrointestinal stromal tumors. *Clin. Cancer Res.* **14,** 12285–12294 (2008).
32. Bougherara, H. *et al.* The aberrant localization of oncogenic kit tyrosine kinase receptor mutants is reversed on specific inhibitory treatment. *Mol. Cancer Res.* **7,** 1525–1533 (2009).
33. Jahn, T. *et al.* Analysing c-kit internalization using a functional c-kit-EGFP chimera containing the fluorochrome within the extracellular domain. *Oncogene* **21,** 4508–4520 (2002).
34. Kon, S. *et al.* Smap1 deficiency perturbs receptor trafficking and predisposes mice to myelodysplasia. *J. Clin. Invest.* **123,** 1123–1137 (2013).
35. Mercer, J. & Helenius, A. Virus entry by macropinocytosis. *Nat. Cell Biol.* **11,** 510–520 (2009).
36. Naal, R. M., Holowka, E. P., Baird, B. & Holowka, D. Antigen-stimulated trafficking from the recycling compartment to the plasma membrane in RBL mast cells. *Traffic* **4,** 190–200 (2003).
37. Sigismund, S. *et al.* Clathrin-mediated internalization is essential for sustained EGFR signaling but dispensable for degradation. *Dev. Cell* **15,** 209–219 (2008).
38. Di Guglielmo, G. M., Le Roy, C., Goodfellow, A. F. & Wrana, J. L. Distinct endocytic pathways regulate TGF-beta receptor signalling and turnover. *Nat. Cell Biol.* **5,** 410–421 (2003).
39. Sigismund, S. *et al.* Endocytosis and signaling: cell logistics shape the eukaryotic cell plan. *Physiol. Rev.* **92,** 273–366 (2012).
40. Heuser, J. E. & Anderson, R. G. Hypertonic media inhibit receptor-mediated endocytosis by blocking clathrin-coated pit formation. *J. Cell Biol.* **108,** 389–400 (1989).
41. von Kleist, L. *et al.* Role of the clathrin terminal domain in regulating coated pit dynamics revealed by small molecule inhibition. *Cell* **146,** 471–484 (2011).
42. Orlandi, P. A. & Fishman, P. H. Filipin-dependent inhibition of cholera toxin: evidence for toxin internalization and activation through caveolae-like domains. *J. Cell Biol.* **141,** 905–915 (1998).
43. Acconcia, F., Sigismund, S. & Polo, S. Ubiquitin in trafficking: The network at work. *Exp. Cell Res.* **315,** 1610–1618 (2009).
44. Hayer, A. *et al.* Caveolin-1 is ubiquitinated and targeted to intralumenal vesicles in endolysosomes for degradation. *J. Cell Biol.* **191,** 615–629 (2010).
45. Yee, N. S., Hsiau, C. W., Serve, H., Vosseller, K. & Besmer, P. Mechanism of down-regulation of c-kit receptor. Roles of receptor tyrosine kinase, phosphatidylinositol 3′-kinase, and protein kinase C. *J. Biol. Chem.* **269,** 31991–31998 (1994).
46. Stuffers, S., Wegner, S. C., Stenmark, H. & Brech, A. Multivesicular endosome biogenesis in the absence of ESCRTs. *Traffic* **10,** 925–937 (2009).
47. Mali, R. S. *et al.* Rho kinase regulates the survival and transformation of cells bearing oncogenic forms of KIT, FLT3, and BCR-ABL. *Cancer Cell* **20,** 357–369 (2011).
48. Joly, M., Kazlauskas, A., Fay, F. S. & Corvera, S. Disruption of PDGF receptor trafficking by mutation of its PI-3 kinase binding sites. *Science* **263,** 684–687 (1994).
49. Er, E. E., Mendoza, M. C., Mackey, A. M., Rameh, L. E. & Blenis, J. AKT facilitates EGFR trafficking and degradation by phosphorylating and activating PIKfyve. *Sci. Signal* **6,** ra45 (2013).
50. Ménard, L., Parker, P. J. & Kermorgant, S. Receptor tyrosine kinase c-Met controls the cytoskeleton from different endosomes via different pathways. *Nat. Commun.* **5,** 3907 (2014).
51. Wang, Y., Pennock, S. D., Chen, X., Kazlauskas, A. & Wang, Z. Platelet-derived growth factor receptor-mediated signal transduction from endosomes. *J. Biol. Chem.* **279,** 8038–8046 (2004).
52. Sun, Y., Hedman, A. C., Tan, X., Schill, N. J. & Anderson, R. A. Endosomal type Iγ PIP 5-kinase controls EGF receptor lysosomal sorting. *Dev. Cell* **25,** 144–155 (2013).
53. Kim, M. S., Rådinger, M. & Gilfillan, A. M. The multiple roles of phosphoinositide 3-kinase in mast cell biology. *Trends Immunol.* **29,** 493–501 (2008).
54. Várnai, P. & Balla, T. Visualization of phosphoinositides that bind pleckstrin homology domains: calcium- and agonist-induced dynamic changes and relationship to myo-[3H]inositol-labeled phosphoinositide pools. *J. Cell Biol.* **143,** 501–510 (1998).
55. Clague, M. J., Urbé, S., Aniento, F. & Gruenberg, J. Vacuolar ATPase activity is required for endosomal carrier vesicle formation. *J. Biol. Chem.* **269,** 21–24 (1994).
56. Griffiths, G., Quinn, P. & Warren, G. Dissection of the Golgi complex. I. Monensin inhibits the transport of viral membrane proteins from medial to trans Golgi cisternae in baby hamster kidney cells infected with Semliki Forest virus. *J. Cell Biol.* **96,** 835–850 (1983).
57. Helenius, A. & Aebi, M. Roles of N-linked glycans in the endoplasmic reticulum. *Annu. Rev. Biochem.* **73,** 1019–1049 (2004).
58. Klausner, R. D., Donaldson, J. G. & Lippincott-Schwartz, J. Brefeldin A: insights into the control of membrane traffic and organelle structure. *J. Cell Biol.* **116,** 1071–1080 (1992).
59. Schmidt-Arras, D. *et al.* Oncogenic deletion mutants of gp130 signal from intracellular compartments. *J. Cell Sci.* **127,** 341–353 (2014).
60. Kazi, J. U., Agarwal, S., Sun, J., Bracco, E. & Rönnstrand, L. Src-like-adaptor protein (SLAP) differentially regulates normal and oncogenic c-Kit signaling. *J. Cell Sci.* **127,** 653–662 (2014).
61. Cremona, O. *et al.* Essential role of phosphoinositide metabolism in synaptic vesicle recycling. *Cell* **99,** 179–188 (1999).
62. Shin, H. W. *et al.* An enzymatic cascade of Rab5 effectors regulates phosphoinositide turnover in the endocytic pathway. *J. Cell Biol.* **170,** 607–618 (2005).
63. Rong, Y. *et al.* Clathrin and phosphatidylinositol-4,5-bisphosphate regulate autophagic lysosome reformation. *Nat. Cell Biol.* **14,** 924–934 (2012).
64. Sridhar, S. *et al.* The lipid kinase PI4KIIIβ preserves lysosomal identity. *EMBO J.* **32,** 324–339 (2013).
65. Bandi *et al.* E3 ligase-defective Cbl mutants lead to a generalized mastocytosis and myeloproliferative disease. *Blood* **114,** 4197–4208 (2009).
66. Zeng, S., Xu, Z., Lipkowitz, S. & Longley, J. B. Regulation of stem cell factor receptor signaling by Cbl family proteins (Cbl-b/c-Cbl). *Blood* **105,** 226–232 (2005).
67. Zermati, Y. *et al.* Effect of tyrosine kinase inhibitor STI571 on the kinase activity of wild-type and various mutated c-kit receptors found in mast cell neoplasms. *Oncogene* **22,** 660–664 (2003).
68. Bauer, S., Duensing, A., Demetri, G. D. & Fletcher, J. A. KIT oncogenic signaling mechanisms in imatinib-resistant gastrointestinal stromal tumor: PI3-kinase/AKT is a crucial survival pathway. *Oncogene* **26,** 7560–7568 (2007).
69. Edris *et al.* Anti-KIT monoclonal antibody inhibits imatinib-resistant gastrointestinal stromal tumor growth. *Proc. Natl Acad. Sci. USA* **110,** 3501–3506 (2013).
70. Scaltriti *et al.* Lapatinib, a HER2 tyrosine kinase inhibitor, induces stabilization and accumulation of HER2 and potentiates trastuzumab-dependent cell cytotoxicity. *Oncogene* **28,** 803–814 (2009).

Acknowledgements

We thank Dr Hirohisa Saito and Dr Kenji Matsumoto (National Center for Child Health and Development) for providing HMC-1 cells, Dr Ko Okumura (Juntendo University) for RBL-2H3 cells, Dr Ryo Goitsuka (Tokyo University of Science) for pt18 cells, Dr Hajime Karasuyama (Tokyo Medical and Dental University) for the pBCMGS vector, Dr Masayuki Oda (Kyoto Prefectural University) for the GST-SH2 expression vector, Dr Tamás Balla (National Institutes of Health) for the PH-GFP expression vector and Dr Toshinori Nakayama (Chiba University) for an anti-phosphotyrosine antibody. We are grateful to Dr Daijiro Sugiyama (Daiichi-Sankyo), Dr Takachika Azuma and Dr Yasushi Hara (Tokyo University of Science) for their helpful advice and sharing of materials throughout this study. This work was supported by a grant-in-aid for Scientific Research from the Japanese Ministry of Education, Culture, Sports, Science and Technology to R.A., and a research grant from the NOVARTIS FOUNDATION (Japan) for the Promotion of Science.

Author contributions

Y.O. conceived, designed, performed and analysed data from all experiments, and wrote the paper. S.T. and E.W. characterized R cells as mast-like cells *in vivo* and *in vitro* by flow cytometry, histo-cytochemical staining, electron microscopy, proliferation assays and microarray analyses, and edited the manuscript. S.S. and S.O performed immunoblotting, immunoprecipitation assays, *in vitro* GST-pulldown assays and RNA interference experiments. H.E. advised on the design of the *in vitro* experiments and edited the manuscript. R.A. conceived and supervised the project, analysed data and wrote the manuscript.

Additional information

Supplementary Information accompanies this paper at http://www.nature.com/naturecommunications

Competing financial interests: The authors declare no competing financial interests.

Reprints and permission information is available online at http://npg.nature.com/reprintsandpermissions/

How to cite this article: Obata, Y. *et al.* Oncogenic Kit signals on endolysosomes and endoplasmic reticulum are essential for neoplastic mast cell proliferation. *Nat. Commun.* 5:5715 doi: 10.1038/ncomms6715 (2014).

⌘ *Author's Choice*

THE JOURNAL OF BIOLOGICAL CHEMISTRY VOL. 289, NO. 30, pp. 20813–20823, July 25, 2014

Epidermal Growth Factor Receptor (EGFR) Signaling Regulates Global Metabolic Pathways in EGFR-mutated Lung Adenocarcinoma*[S]

Received for publication, April 21, 2014, and in revised form, June 9, 2014 Published, JBC Papers in Press, June 13, 2014, DOI 10.1074/jbc.M114.575464

Hideki Makinoshima[‡1], Masahiro Takita[‡§], Shingo Matsumoto[‡¶], Atsushi Yagishita[‡], Satoshi Owada[‖], Hiroyasu Esumi[‖], and Katsuya Tsuchihara[‡§]

From the [‡]Division of Translational Research, Exploratory Oncology Research & Clinical Trial Center, National Cancer Center, Kashiwa, Chiba 277-8577, Japan, [§]Department of Integrated Biosciences, Graduate School of Frontier Sciences, The University of Tokyo, Kashiwa, Chiba 277-8561, Japan, [¶]Thoracic Oncology Division, National Cancer Center Hospital East, Kashiwa, Chiba 277-8577, Japan, and [‖]Research Institute for Biomedical Sciences, Tokyo University of Science, Noda, Chiba 278-0022, Japan

Background: Genetic mutations in cancer-driver genes induce specific metabolic alterations in cancer cells.
Results: EGF receptor signaling has an important role for glycolysis, pentose phosphate pathway, and pyrimidine biosynthesis in EGFR-mutated lung cancer.
Conclusion: Our work reveals the relationship between the EGFR signaling axis and key metabolic changes.
Significance: These data implicate a possible link between therapeutic response and regulation of metabolism in EGFR-mutated LAD.

Genetic mutations in tumor cells cause several unique metabolic phenotypes that are critical for cancer cell proliferation. Mutations in the tyrosine kinase epidermal growth factor receptor (EGFR) induce oncogenic addiction in lung adenocarcinoma (LAD). However, the linkage between oncogenic mutated EGFR and cancer cell metabolism has not yet been clearly elucidated. Here we show that EGFR signaling plays an important role in aerobic glycolysis in EGFR-mutated LAD cells. EGFR-tyrosine kinase inhibitors (TKIs) decreased lactate production, glucose consumption, and the glucose-induced extracellular acidification rate (ECAR), indicating that EGFR signaling maintained aerobic glycolysis in LAD cells. Metabolomic analysis revealed that metabolites in the glycolysis, pentose phosphate pathway (PPP), pyrimidine biosynthesis, and redox metabolism were significantly decreased after treatment of LAD cells with EGFR-TKI. On a molecular basis, the glucose transport carried out by glucose transporter 3 (GLUT3) was downregulated in TKI-sensitive LAD cells. Moreover, EGFR signaling activated carbamoyl-phosphate synthetase 2, aspartate transcarbamylase, and dihydroorotase (CAD), which catalyzes the first step in *de novo* pyrimidine synthesis. We conclude that EGFR signaling regulates the global metabolic pathway in EGFR-mutated LAD cells. Our data provide evidence that may link therapeutic response to the regulation of metabolism, which is an attractive target for the development of more effective targeted therapies to treat patients with EGFR-mutated LAD.

The discovery of oncogenic driver mutations allows us to identify druggable targets and develop new therapies using small molecule tyrosine kinase inhibitors (TKIs)[2] aimed at the relevant patient populations (1–3). More than 50% of lung adenocarcinomas (LAD) from East Asian non-smokers harbor EGFR mutations, and these tumors have been termed oncogene addicted to reflect their dependence on EGFR-mediated pro-survival signaling and their high susceptibility to apoptosis induced by EGFR-TKIs (*e.g.* gefitinib and erlotinib) (4–7). The tyrosine kinase activity of EGFR is dysregulated by gene mutations that lead to aberrant EGFR signaling through pathways including the RAS/MAPK and PI3K/AKT pathways (8, 9). The most frequently occurring mutations in the *EGFR* gene (in-frame deletion in exon 19 at codons 746–750 or a single-base substitution L858R in exon 21) predict an improved clinical response to first-line oral EGFR-TKIs compared with standard platinum-based chemotherapy in patients with advanced non-small-cell lung carcinoma (NSCLC) (4, 8).

There is accumulating evidence that genetic mutations in cancer-driver genes, tumor suppressors, and amplified oncogenes are linked to specific alterations in metabolic activity in cancer cells, involving proteins such as isocitrate dehydrogenase (IDH), fumarate hydratase (FH), MYC, K-RAS, and BRAF (10–13). The Warburg effect, the phenomenon in which cancer cells exhibit rapid glucose consumption with secretion of lactate despite abundant oxygen availability, has been recognized since the 1930s (14–16). Indeed, glucose metabolism in cancer cells is tightly regulated by many molecules at the transcriptional, translational, and post-translational levels (10, 17, 18). c-MYC is critically involved in the regulation of many growth-

* This work was supported by the National Cancer Center Research and Development Fund (25-A-6) and JSPS KAKENHI Grant Number 24300345 (to K. T.).
[S] This article contains supplemental Tables S1 and S2.
⌘ *Author's Choice*—Final version full access.
[1] To whom correspondence should be addressed: Division of Translational Research, Exploratory Oncology Research & Clinical Trial Center, National Cancer Center, Kashiwa, Chiba 277-8577, Japan. Tel.: 81-4-7134-6855; Fax: 81-4-7134-6865; E-mail: hmakinos@east.ncc.go.jp.

[2] The abbreviations used are: TKI, tyrosine kinase inhibitor; EGFR, epidermal growth factor receptor; LAD, lung adenocarcinoma; IC_{50}, half maximal inhibitory concentration; PPP, pentose phosphate pathway; ECAR, extracellular acidification rate; OCR, oxygen consumption rate; GLUT, glucose transporter; CAD, carbamoyl-phosphate synthetase 2, aspartate transcarbamylase, and dihydroorotase.

promoting signal transduction pathways and glucose metabolism genes, including GLUT1, hexokinase 2 (HK2), pyruvate kinase muscle (PKM2), and lactate dehydrogenase A (LDHA) (10, 19). Through the up-regulation of these genes, c-MYC contributes directly to the Warburg effect (19). The enzymatic activities of glycolytic enzymes such as HK2, phosphofructokinase (PFK), PKM2, and LDHA are modulated by post-translational modification (18). For example, PKM2 is phosphorylated in its tyrosine residue (Y105) with low activity in human cancer cells, resulting in increased lactate production, which is one-step downstream from PKM2 in glycolysis, even under aerobic conditions (14, 17). Furthermore, PKM2 promotes the Warburg effect through EGF-stimulated EGFR activation and the MAPK signaling pathway (20, 21). In brain cancer, the activating EGFRvIII mutation induces enhanced glycolysis by promoting glycolytic gene expression through the Myc/Max pathway (22). However, the specific role of mutated EGFR for aerobic glycolysis in lung cancer has not yet been clearly described.

In this work, we demonstrate that EGFR signaling is required for lactate production under aerobic growth conditions in LAD cells. EGFR signaling maintains key metabolites in glycolysis and PPP by regulating glucose transport through GLUT3 expression. In addition to glucose metabolism, we show that EGFR signaling up-regulates *de novo* pyrimidine biosynthesis. Moreover, we describe the altered metabolic profiles in TKI-sensitive LAD cells in response to erlotinib. Our results imply that EGFR signaling plays a central role in modulating global metabolic pathways in EGFR-mutated LAD.

EXPERIMENTAL PROCEDURES

Materials—Cell lines were purchased from the Immuno-Biological Laboratories (Fujioka, Japan) and American Type Culture Collection (ATCC). RPMI 1640 (R8758 and R1383), phosphate-buffered saline (PBS), 2-deoxy-D-glucose (2DG) were purchased from Sigma-Aldrich. Fetal bovine serum (FBS) was purchased from Biowest (Nuaille, France). Dimethyl sulfoxide (DMSO) and glucose were purchased from Wako Pure Chemicals Industries (Osaka, Japan). Gefitinib and erlotinib were purchased from Santa Cruz Biotechnology (Dallas, TX). Cell Counting Kit-8 was purchased from Dojindo Laboratories (Kumamoto, Japan). Lactate assay kit II and glucose assay kit II were purchased from BioVision (Milpitas). FluxPak XF24 assay pack and XF glycolysis stress test kit were purchased from Seahorse Bioscience (North Billerica). Countess Automated Cell Counter including Trypan Blue and chamber slides was purchased from Invitrogen (Carlsbad, CA). Primary antibodies specific for EGFR, phospho-EGFR Tyr-1068, AKT, phospho-AKT Ser473, ERK1/2, phospho-ERK1/2 Thr202/Tyr204, GSK3α/β, phospho-GSK3α/β Ser21/9, c-MYC, PKM2, phospho-PKM2 Tyr105, GYS, phospho-GYS Ser641, LDHA, phospho-LDHA Tyr-15, HK2, S6K, phospho-S6K Thr421/Ser424, CAD, phospho-CAD (Ser-1859), and β-actin were purchased from Cell Signaling Technologies (Danvers, MA) and GLS, GLUT1, GLUT3, PDHA1, and phospho-PDHA1 Ser-293 from Abcam (Cambridge, UK), respectively. The peroxidase-linked secondary antibodies for WB, HRP-linked Sheep anti-mouse IgG and Donkey anti-rabbit IgG, were purchased from GE Healthcare Biosciences (Pittsburgh, PA). Fluorescein (FITC)-conjugated goat anti-rabbit IgG for FACS was purchased from Beckman Coulter (Fullerton, CA). Oligomycin was purchased from Merck Millipore (Darmstadt, Germany). SYBR Premix Ex Taq was purchased from TaKaRa Bio (Shiga, Japan). Ribonuclease A (RNase A) was purchased from Roche Applied Science (Penzberg, Germany) and contaminated DNase was inactivated at 80 °C for 30 min. 3-*O*-(^{3}H-methyl)-*D*-glucose (3-OMeG) was purchased from Perkin Elmer (Waltham, MA).

Cell Survival Assay and Proliferation Assay—EGFR mutant LAD cells were seeded in RPMI 1640 containing various concentrations of EGFR inhibitors in 96-well cell culture plates. After 72 h of incubation, cell viability was analyzed using a WST-8 assay using the Cell Counting Kit-8 (Dojindo, Japan). To count the number of viable cells, Trypan Blue-negative cells were counted using a Countess Automated Cell Counter (Invitrogen).

Lactate and Glucose Assay—Lactate and glucose in culture medium were measured with the respective lactate assay kit II and glucose assay kit II according to the manufacturer's instructions (BioVision, Mountain View, CA). Briefly, after centrifugation (3,500 rpm, 15 min, 4 °C), cell culture medium supernatants were frozen at −20 °C. Samples were later thawed, diluted in assay buffer, and mixed with lactate or glucose reaction mixture for 30 min. The optical density of the mixture in each well was read at 450 nm on a microplate reader (Molecular Devices). The lactate concentration was calculated from a standard curve and normalized to cell numbers and culture time. Glucose consumption was calculated from a standard curve, subtracting background from cell-free medium, and normalizing to cell numbers and time.

Measurement of ECAR and OCR—ECAR and OCR were measured with a XF glycolysis stress test kit according to the manufacturer's instructions (Seahorse Bioscience). In brief, 4.5×10^4 cells were plated onto XF24 plates in RPMI 1640 (10% FBS, 2 mM glutamine) and incubated at 37 °C, 5% CO_2 overnight. Cells were washed with assay medium (minus glucose and unbuffered RPMI 1640 (SIGMA R1383)), replaced with assay medium, and then placed at 37 °C in a CO_2-free incubator for 30 min. ECAR and OCR were monitored using a Seahorse Bioscience XF24 Extracellular Flux Analyzer over time and each cycle consisted of 3 min mixing, 3 min waiting and 3 min measuring. Glucose, oligomycin, and 2DG were diluted into XF24 media and loaded into the accompanying cartridge to achieve final concentrations of 10 mM, 5 μM, and 100 mM, respectively. Injections of the drugs into the medium occurred at the time points specified.

Western Blotting—Cells were lysed in RIPA buffer (150 mM NaCl, 1% Triton X-100, 0.5% sodium deoxycholate, 0.1% SDS, 50 mM Tris, pH 8.0) on ice for 10 min, sonicated, and centrifuged at 15,000 × *g* for 10 min. The protein content of supernatants was measured by BCA assay (Pierce). Identical amounts of protein samples were separated via 4–20% SDS/PAGE, transferred to PVDF membranes, and incubated overnight with primary antibodies (1:1000 dilution). The primary antibodies used in this study are listed in the materials. ECL anti-rabbit IgG HRP-linked whole antibody (1:10,000; GE Healthcare) and ECL anti-mouse IgG HRP-linked whole antibody (1:10,000; GE Healthcare) were used as secondary antibodies. Signals were

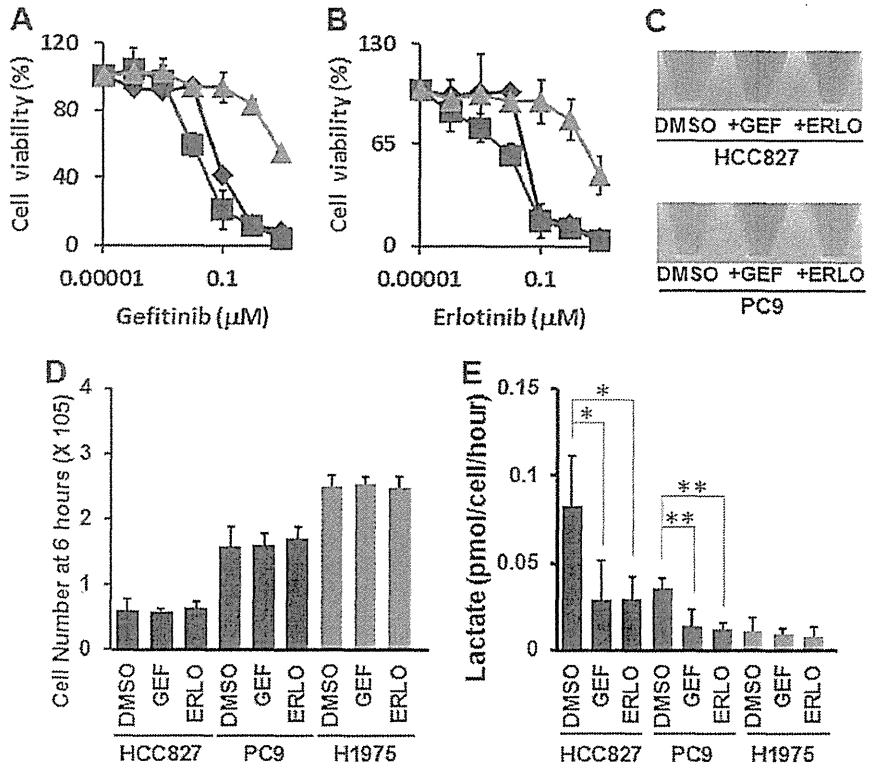

FIGURE 1. **EGFR-TKI treatment represses lactate production in TKI-sensitive LAD cells.** *A*, WST-8 assay with gefitinib. Cells were treated with the indicated inhibitors for 72 h, and the viability was assessed by the WST-8 assay. Data are shown as the mean ± S.D. ($n = 6$). *Blue line*: HCC827, *red line*: PC-9, *green line*: H1975. The *in vitro* half-maximal inhibitory concentration (IC_{50}) for the growth of EGFR-mutated LAD cell lines was determined such that HCC827 to gefitinib: 0.085 μM, PC-9 to gefitinib: 0.031 μM, and H1975 to gefitinib: >10 μM. *B*, WST-8 assay with erlotinib. Cells were treated with the indicated concentrations for 72 h, and viability was assessed by the WST-8 assay. The data are shown as the mean ± S.D. ($n = 6$). *Blue line*: HCC827, *red line*: PC-9, *green line*: H1975. The *in vitro* half-maximal inhibitory concentration (IC_{50}) for the growth of EGFR-mutated LAD cell lines was determined such that HCC827 to 0.065 μM, PC-9 to 0.067 μM and H1975 to 8.8 μM. *C*, medium color in HCC827 and PC-9 was altered by addition of EGFR-TKIs (1 μM) for 24 h. The phenol red in culture media exhibits a gradual color transition from red to yellow over the pH range 8.0 to 6.6. *D*, cell growth responses at 6 h to 1 μM of gefitinib or erlotinib were measured using a Trypan Blue staining. The cell number of HCC827 (*blue*), PC-9 (*red*), and H1975 were shown. GEF; gefitinib, ERLO; erlotinib. The data are shown as the mean ± S.D. ($n = 4$). *, $p < 0.05$; **, $p < 0.01$ *versus* control by two-tailed Student's *t* test. *E*, extracellular lactate production in HCC827 (*blue*), PC-9 (*red*) and H1975 (*green*) cell lines at 6 h post-TKI treatment. Error bars indicate S.D. ($n = 6$). *, $p < 0.05$; **, $p < 0.01$ *versus* control by two-tailed Student's *t* test.

detected using ECL Western blotting detection reagent (GE Healthcare) and x-ray films (GE Healthcare).

Quantitative RT-PCR—Cells were washed with PBS and total RNA from the LAD cell lines was isolated with TRIzol Reagent (Invitrogen). Complementary DNA (cDNA) was synthesized using the SuperScript VILO cDNA synthesis kit (Invitrogen). Synthesized primers were purchased from TaKaRa Bio (Japan). Real-time RT-PCR was carried out with specific primers and a 7500 detection system (Applied Biosystems). β-Actin was used for normalization as control and the relative quantitation value compared with the calibrator for that target is expressed as $2^{-(Ct-Cc)}$.

Metabolite Measurements—Metabolic extracts were prepared from 2–5 × 10^6 cells with methanol containing Internal Standard Solution (Human Metabolome Technologies; HMT, Inc., Tsuruoka, Japan) and analyzed using a capillary electrophoresis (CE)-connected ESI-TOFMS and CE-MS/MS system (HMT, CARCINOSCOPE). 2–5 × 10^6 cells were used for the extraction of intracellular metabolites. Culture medium was removed from the dish, and cells were washed twice in 5% mannitol solution (10 ml first and then 2 ml). Cells were then treated with 800 μl of methanol and 550 μl of Milli-Q water containing internal standards (H3304–1002, HMT, Inc., Tsuruoka, Japan). The metabolite extract was transferred into a microfuge tube and centrifuged at 2,300 × *g* and 4 °C for 5 min. Next, the upper aqueous layer was centrifugally filtered through a Millipore 5-kDa cutoff filter at 9,100 × *g* and 4 °C for 120 min to remove proteins. The filtrate was centrifugally concentrated and resuspended in 50 μl of Milli-Q water for CE-MS analysis. Cationic compounds were analyzed in the positive mode of CE-TOFMS and anionic compounds were analyzed in the positive and negative modes of CE-MS/MS according to the methods developed by Soga *et al.* (23–25). To obtain peak information including *m/z*, migration time (MT), and peak area, detected peaks by CE-TOFMS and CE-MS/MS were extracted using automatic integration software (MasterHands, Keio University, Tsuruoka, Japan and MassHunter Quantitative Analysis B.04.00, Agilent Technologies, Santa Clara, CA, respectively). The peaks were annotated with putative metabolites from the HMT metabolite database based on their MTs in CE and *m/z* values determined by TOFMS. The tolerance range for the peak annotation was configured at ±0.5 min for MT and ±10 ppm for *m/z*. In addition, concentrations of metabolites were calculated by normalizing the peak area of each metabolite with respect to the area of the internal standard and by using standard curves, which were obtained by three-point calibrations.

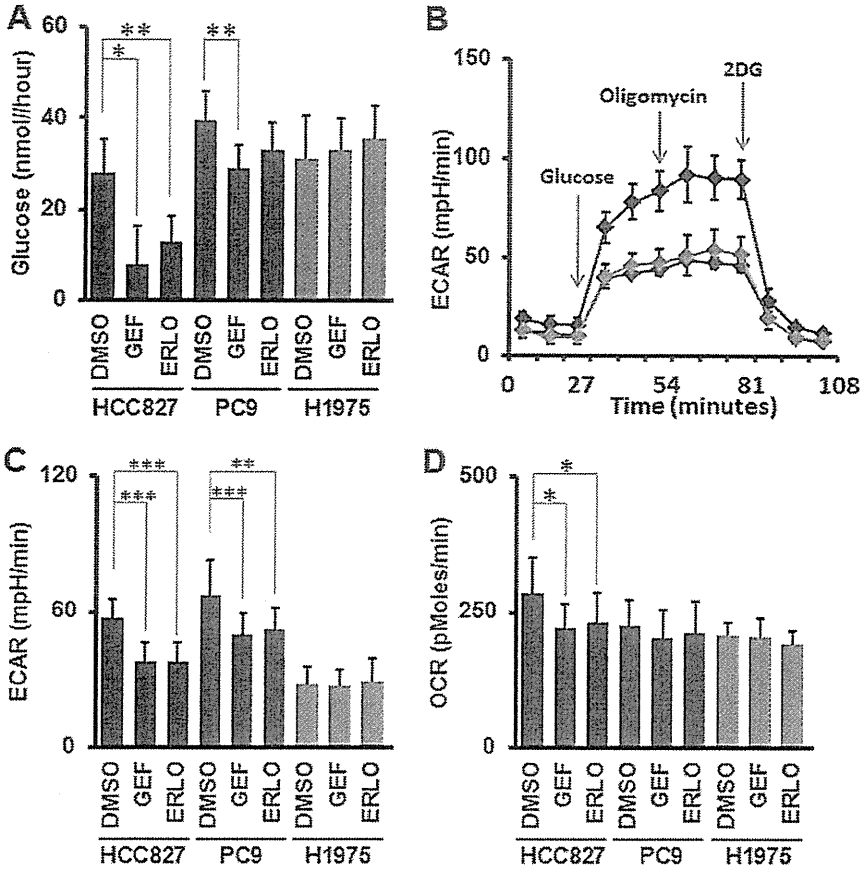

FIGURE 2. **Glucose consumption and flux analysis monitoring glucose metabolism.** *A*, glucose consumption rate in HCC827 (*blue*), PC-9 (*red*), and H1975 (*green*) cells. Cells were cultured for 24 h in the absence or presence of EGFR-TKIs and glucose concentration in culture supernatant was quantified. Cell-free medium was used as a background control. Error bars indicate S.D. ($n = 6$). *, $p < 0.05$; **, $p < 0.01$ *versus* control by two-tailed Student's *t* test. *B*, measurement of ECAR over time. After 6-h treatment with TKIs, cells were applied to flux assay. ECAR was measured every 9 min. The addition of glucose, oligomycin, and 2-deoxy-D-glucose (*2DG*) was carried out at the time point indicated by the *arrows*. Error bars indicate S.D. *C*, ECAR values of HCC827 (*blue*), PC-9 (*red*), and H1975 (*green*) cells at 36 min of flux assay. Error bars indicate S.D. ($n = 24$–30). **, $p < 0.005$; ***, $p < 0.001$ *versus* control by two-tailed Student's *t* test. All cells were treated with the indicated TKIs (1 μM) for 6 h before each assay. *GEF*, gefitinib; *ERLO*, erlotinib. *D*, OCR values of HCC827 (*blue*), PC-9 (*red*), and H1975 (*green*) cells at 36 min of flux assay. Error bars indicate S.D. ($n = 24$–30). *, $p < 0.001$ *versus* control by two-tailed Student's *t* test. All cells were treated with the indicated TKIs (1 μM) for 6 h before each assay. *GEF*, gefitinib; *ERLO*, erlotinib.

Expression of Glucose Transporter and Glucose Transport Assay—To detect expression of membrane-bound GLUTs, cells were fixed with 80% ethanol and incubated with anti-GLUT3 antibody (Abcam) and stained with the appropriate FITC-conjugated anti-rabbit IgG antibody (Jackson Immuno Research). Quantification of FITC-fluorescent intensity was performed using a FACSCanto II (BD Biosciences). Procedures for 3-OMeG uptake assay were previously described (26). LAD cells were treated with indicated TKIs for 6 h before glucose transport assay. Uptake was performed from 0.5 min to 10 min and radioactivity in the cells was quantified with Tri-Carb 3110TR low activity liquid scintillation analyzer (PerkinElmer).

Statistical Analyses—Unless otherwise indicated, results were reported as the mean ± S.D. Statistical analyses were done by two-tailed Student's *t* test. For metabolomic data analysis we used Welch *t* test and *p* values were indicated as *, <0.05; **, <0.01; and ***, <0.001.

RESULTS

Lactate Production Was Decreased in TKI-sensitive LAD Cells after EGFR-TKI Treatment—We initially characterized the EGFR-mutated lung adenocarcinoma cell lines used in this study by measuring cell viability in the absence or presence of EGFR-TKIs after 72 h. All three LAD cell lines have the EGFR mutation in either exon 19 or exon 21. Cell line HCC827 carried the delE746-A750 mutation, PC-9 exhibited delE746-A750 and NCI-H1975 (H1975) carried EGFR L858R+T790M (27, 28). The H1975 cells have the T790M mutation, which causes resistance to gefitinib and erlotinib (29). HCC827 and PC-9 cell lines were highly sensitive to the EGFR-TKI gefitinib and erlotinib in the nanomolar range as compared with the TKI-resistant cell H1975 (Fig. 1, *A* and *B*). These data are consistent with previous findings (27, 28, 30).

In dose response assays with EGFR inhibitors, we observed differences in the color of the culture medium in the presence of TKIs against EGFR, especially in the growth cultures of TKI-sensitive cell lines (Fig. 1*C*). In culture media, phenol red exhibits a gradual color transition from red to yellow at lower pH values as a result of lactate production (31). Therefore, we explored the glycolytic capacity of EGFR-mutated LAD cells. Since a 72-h incubation with TKIs leads to a dramatic reduction in cell viability in sensitive cell lines, we set up experimental conditions where TKI treatment was given at a relatively higher concentration (1 μM) and

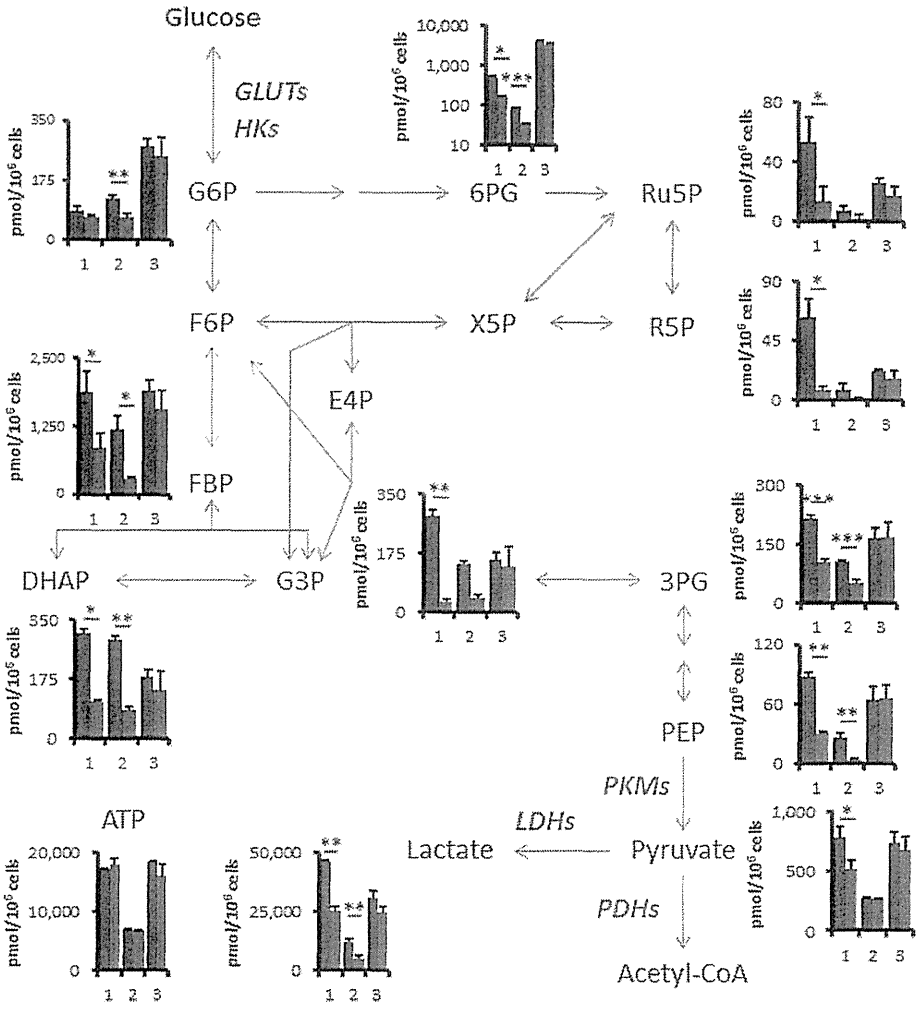

FIGURE 3. **EGFR signaling up-regulates glycolysis and the pentose phosphate pathway.** Intracellular concentration (pmol/million cells) of key metabolites involved in glycolysis and pentose phosphate pathway (*PPP*) after the inhibition of EGFR signaling is shown. Error bars indicate S.D. ($n = 3$). Total metabolites were extracted with methanol from HCC827, PC9 or H1975 cells treated with DMSO (*blue*) or erlotinib (*red*, 1 μM) for 6 h. Representative metabolites such as glucose 6-phosphate (*G6P*), fructose 1,6-bisphosphate (*FBP*), glyceraldehyde 3-phosphate (*G3P*), dihydroxyacetone phosphate (*DHAP*), 3-phosphoglycerate (*3PG*), phosphoenolpyruvate (*PEP*), pyruvate (*PA*), lactate (*LA*), 6-phosphogluconate (*6PG*), ribulose 5-phosphate (*Ru5P*), ribose 5-phosphate (*R5P*), and ATP are shown here. Others are listed in supplemental Table 1.

shorter time (6 h) to allow all cells to grow equally and thereby standardize the number of viable cells analyzed (Fig. 1*D*). Interestingly, we discovered that exposure of the cells to TKIs for up to 6 h significantly lowered the rate of lactate accumulation in the medium of TKI-sensitive LAD cell lines but not in resistant cells (Fig. 1*E*, *, $p < 0.05$; **, $p < 0.01$ *t* test).

Glycolytic Activities Were Down-regulated in TKI-sensitive LAD Cells after Inhibition of EGFR Signaling—Next, we quantified the glucose consumption rate and found that inhibition of EGFR signaling significantly lowered the rate of glucose consumption from the growth medium of TKI-sensitive HCC827 and PC9 cells but not in the TKI-resistant H1975 cells (Fig. 2*A* *, $p < 0.05$; **, $p < 0.01$ *t* test).

To better define lactate production derived from glucose, we measured the glucose-induced extracellular acidification rate (ECAR), an indicator of lactate production, and the oxygen consumption rate (OCR), an indicator of oxidative phosphorylation (OXPHOS), using a flux analyzer. Basal levels of ECAR at the beginning of measurements, which indicated non-glycolytic acidification, were low in HCC827 cells (Fig. 2*B*). Equivalent ECAR was observed in HCC827 cells both pre- and post-treatment with an ATPase inhibitor oligomycin to induce maximum cellular glycolytic capacity (Fig. 2*B*). At the final step, the addition of 2-deoxy-D-glucose (2DG), an inhibitor for glycolysis, completely shut down extracellular acidification (Fig. 2*B*). ECAR was statistically higher in DMSO controls compared with TKI-treated HCC827 and PC-9 cells (Fig. 2*C* *, $p < 0.01$; **, $p < 0.005$; ***, $p < 0.001$ *t* test). In contrast to ECAR, OCR was changed in TKI-treated HCC827, but not in PC-9 and H1975 cells (Fig. 2*D*).

EGFR Signaling Up-regulates Glycolysis and the Pentose Phosphate Pathway—To confirm the reduction of glycolysis metabolites by TKIs, we extracted intracellular metabolites with methanol and analyzed using capillary electrophoresis time-of-flight mass spectrometry (CE-TOFMS) (25). Metabolome analysis revealed that intermediate metabolites in glycolysis and the pentose phosphate pathway (PPP) were down-regulated by erlotinib treatment for 6 h in both HCC827 and PC-9

cells (Fig. 3 and supplemental Table S1). We observed that key glycolysis and PPP metabolites such as fructose 1,6-bisphosphate (FBP), dihydroxyacetone phosphate (DHAP), 3-phosphoglycerate (3PG), phosphoenolpyruvate (PEP), lactate (LA), and 6-phosphogluconate (6PG) were decreased in TKI-sensitive HCC827 and PC9 cells after 6 h of erlotinib treatment, but not in TKI-resistant H1975 cells (Fig. 3 and supplemental Table S1). Glucose 6-phosphate (G6P), glyceraldehyde 3-phosphate (G3P), pyruvate (PA), ribulose 5-phosphate (Ribu5P), and ribose 5-phosphate (R5P) were significantly reduced in both HCC827 and PC9 cells. The amount of adenosine triphosphate (ATP), which is the molecular unit of currency of intracellular energy transfer, was not changed in any of the tested three cell lines after erlotinib treatment. The reduction of glucose utilization after TKI treatment was observed in both glycolysis and pentose phosphate pathways, suggesting that EGFR signaling might regulate a glucose transport or hexokinase activity in TKI-sensitive LAD cells.

MYC-regulated Gene Expression for Glycolytic Enzymes—To test whether EGFR-TKIs inhibited EGFR activity and related signaling molecules under our experimental conditions, we determined levels of total EGFR, phospho-EGFR (p-EGFR), ERK1/2, p-ERK1/2, AKT, p-AKT, MYC, and β-actin in cells treated with DMSO or gefitinib (1 μM) for 2 h by Western blot (WB) analyses. Despite equivalent amounts of total EGFR, p-EGFR was clearly repressed in HCC827 and PC9 cells, but not in H1975 cells (Fig. 4*A*). Downstream signaling molecules such as ERK1/2 and AKT were also inactivated by the addition of gefitinib to HCC827 and PC9 cells as compared with H1975 cells (Fig. 4*A*).

We hypothesized that MYC regulates lactate production through transcriptional regulation, since MYC is an important regulator for cell cycle and glycolysis in cancer cells (19, 32, 33). We found that the levels of MYC were quickly down-regulated at both the mRNA and protein levels in response to EGFR-TKIs (Fig. 4, *A* and *B*). The MYC-regulated genes GLUT1 (glucose transporter 1) and HK2 (Hexokinase 2) were down-regulated in EGFR-TKI sensitive LAD cells, but not in the TKI-resistant H1975 cells (Fig. 4, *C* and *D*). Although previous studies reported that MYC up-regulated PKM2 (pyruvate kinase muscle isozyme 2) (34), we found that the loss of MYC did not affect mRNA expression of PKM2 in HCC827 or PC9 cells (Fig. 4*E*). These data suggest that the reduction of glycolysis after the inhibition of EGFR signaling is caused by down-regulation of the MYC pathway.

Protein Expression and Phosphorylation of Metabolic Enzymes—PKM2 is thought to be a key molecule for aerobic glycolysis in cancer cells (20, 21). We hypothesized that PKM2 might play a critical role in the glycolysis pathway in the response to EGFR-TKI treatment, since PKM2 activity was down-regulated by EGF stimulation resulting in up-regulated lactate production (21). Although the phosphorylation of PKM2 at Tyr-105 was decreased at 24 h after EGFR-TKI addition in TKI-sensitive HCC827 and PC9 cells, this was not seen at the earlier time points (2 or 6 h) post-treatment (Fig. 5*A*). The phosphorylation of PKM2 was not changed in TKI-resistant H1975 cells over time (Fig. 5*A*). Therefore, there may be a more rapid, PKM2-

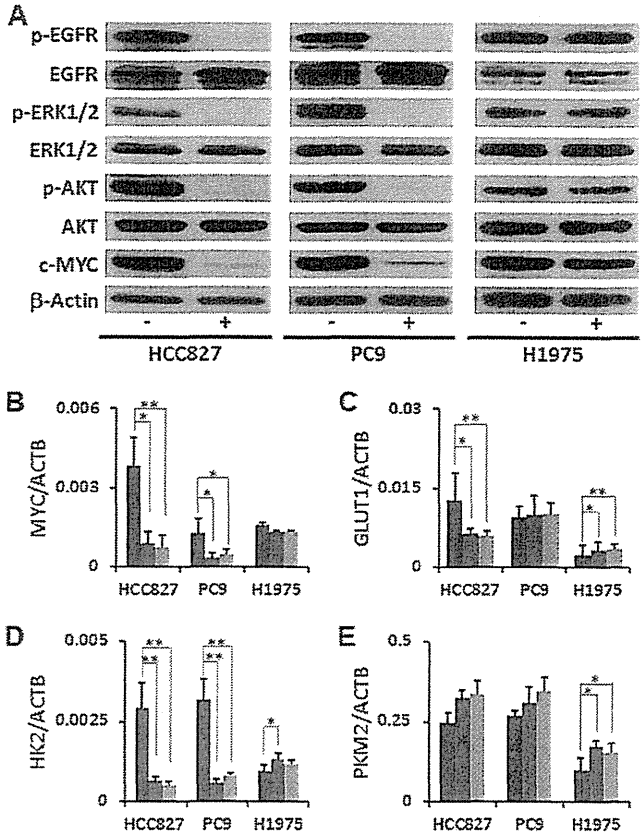

FIGURE 4. **MYC-regulated glycolytic gene expression.** *A*, Western blotting (*WB*) showing proteins related with EGFR signaling. EGFR, phospho-EGFR (*p-EGFR*), ERK1/2, phospho-ERK1/2 (*p-ERK1/2*), AKT, phospho-AKT (*p-AKT*) and c-MYC. Total protein lysates were isolated from the cell treated with gefitinib for 2 h. Equivalent amounts of proteins from whole-cell lysates were subjected to Western blot analysis to detect the indicated proteins. β-Actin was used as a loading control. *B-E*, total RNA was isolated from cells at 6 h post-TKI treatment and analyzed by RT-PCR. *Blue bars* represent DMSO control, *red bars* denote gefitinib treatment, and *green bars* denote erlotinib treatment. The representative genes related with glycolysis are shown here. *MYC*, *GLUT1* (glucose transporter 1, *SLC2A1*), *HK2* (hexokinase 2), and *PKM2* (pyruvate kinase muscle isozyme 2), and others were listed in supplemental Table S2. Error bars indicate S. D. ($n = 6$). *, $p < 0.05$; **, $p < 0.01$ *versus* control by two-tailed Student's *t* test.

independent molecular mechanism by which EGFR signaling regulates the glycolysis pathway.

To determine whether the changes in gene expression driven by MYC were associated with modifications of cellular metabolism, we analyzed phosphorylation and expression of EGFR signaling molecules and glycolytic enzymes by Western blot. We confirmed the effect of TKIs on molecular markers of the EGFR signaling cascade (EGFR, AKT, ERK, and c-Myc) in LAD cells incubated in the presence of gefitinib or erlotinib. We observed that phosphorylation of EGFR, AKT, and ERK was inhibited at 6 h after TKI treatment in HCC827 and PC9 cells (Fig. 5*B*). The expression level of enzymes for glucose metabolism such as GLUT1 and HK2 generally showed regulation in mRNA levels but not at the corresponding protein levels (Fig. 5*B*). In contrast, GLUT3 was decreased in HCC827 and PC-9 cells after 6 h treatment with TKIs (Figs. 4*C* and 5*B*). When we examined the expression level of MYC-regulated glutaminase (GLS) and glycogen synthase (GYS), we saw that GLS and p-GYS were modestly down-regulated in HCC827 and PC9

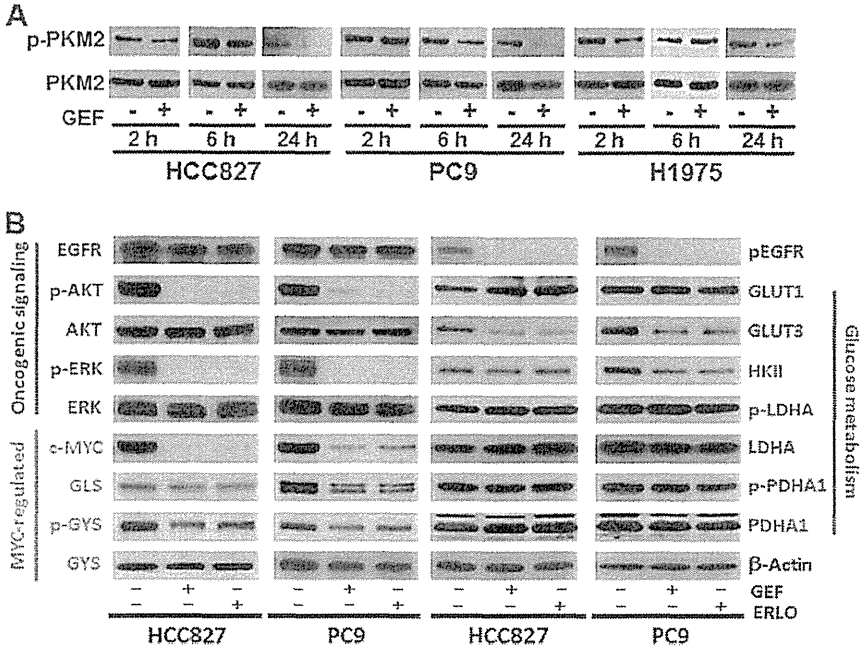

FIGURE 5. **Protein expression and phosphorylation of metabolic enzymes.** *A*, phosphorylation of PKM2 at Tyr-105 is decreased 24 h after EGFR-TKI addition. EGFR inhibition in the TKI-sensitive HCC827 and PC9 cells did not induce significant reduction of phospho-PKM2 at either 2 or 6 h post-treatment. *B*, Western blotting showing proteins related with oncogenic signaling, GLS, GYS, GLUTs, HKII, PDHA1, and phospho-PDHA1. Total protein lysates were isolated from cells treated with gefitinib or erlotinib for 6 h. Equivalent amounts of proteins from whole-cell lysates were subjected to Western blot analysis to detect the indicated proteins. β-Actin was used as a loading control.

(Fig. 5*B*). Lactate dehydrogenase A (LDHA), p-LDHA, pyruvate dehydrogenase α1 (PDHA1), and p-PDHA1 were not altered in HCC827 and PC-9 cells after 6 h treatment with TKIs (Fig. 5*B*).

EGFR Signaling Pathway Down-regulates the Glucose Transporter GLUT3—GLUT1 (glucose transporter 1, *SLC2A1*) and GLUT3 (glucose transporter 3, *SLC2A3*) were mainly expressed in LAD cells (supplemental Table S2). Western blot analysis showed that GLUT3, but not GLUT1, was decreased in HCC827 and PC-9 cells after 6 h of treatment with TKIs. To further confirm membrane-bound GLUT3 expression levels, we investigated the effects of EGFR-TKIs on membrane-bound glucose transporters in HCC827, PC-9, and H1975 cells by flow cytometry. We observed reduction of membrane-bound GLUT3 in the EGFR TKI-sensitive cell lines HCC827 (Fig. 6, *A* and *B*) and PC-9 (Fig. 6, *C* and *D*), although the expression of GLUT3 was unchanged in TKI-resistant H1975 cells (Fig. 6, *E* and *F*) after 6 h of TKI treatment.

To gain additional insight into the functional role of glucose transport, we measured 3-*O*-(^{3}H-methyl)-D-glucose (3-OMeG) uptake in the absence or presence of EGFR-TKIs. Following 6-hr treatment with gefitinib or erlotinib, the 3-OMeG transport rate in HCC827 and PC-9 cells significantly decreased (Fig. 6, *G* and *H*).

Alterations in Additional Metabolic Pathways other than Glycolysis and PPP in the Response to Erlotinib Treatment—To further characterize whether EGFR signaling regulates additional metabolic pathways other than glycolysis and PPP, we quantified metabolites in tricarboxylic acid (TCA), amino acids, and redox. Despite equivalent amount of acetyl-CoA and citrate, fumarate (FA) and malate (MA) were decreased in HCC827 and PC-9 cells but not in H1975 cells after 6 h treatment with erlotinib (Fig. 7*A* and supplemental Table S1). This result suggests that glutaminolysis was down-regulated after inhibition of EGFR signaling, consistent with the lower expression levels of GLS (Fig. 5*B*). In contrast, amino acids such as proline (Pro) and aspartate (Asp) were increased in TKI-sensitive HCC827 and PC9 cells as compared with TKI-resistant H1975 cells (Fig. 7*A* and supplemental Table S1). Additionally, reductive nicotinamide adenine dinucleotide (NADH) and reductive glutathione (GSH) were significantly reduced in HCC827 and PC9 cells, while conversely oxidative glutathione (GSSG) was increased in H1975 cells (Fig. 7*A* and supplemental Table S1).

EGFR Signaling Is Required for de Novo Pyrimidine Biosynthesis—*N*-Carbamoyl-aspartate (NC-Asp) levels were decreased after EGFR-TKI treatment as determined by metabolome analysis (Fig. 7*A*). Consistent with this observation, the phosphorylation of ribosomal protein S6 kinase 1 (S6K) and carbamoyl-phosphate synthetase 2, aspartate transcarbamoylase, dihydroorotase (CAD) were obviously down-regulated in HCC827 and PC9 cells but not in H1975 cells (Fig. 7*B*). The phosphorylation of the Ser1859 residue in CAD protein is required for the first step in the *de novo* synthesis of pyrimidines (35). These data imply that the inhibition of EGFR signaling alters *de novo* pyrimidine biosynthesis in EGFR-mutated LAD cells.

DISCUSSION

In this report, we demonstrated that EGFR signaling up-regulated aerobic glycolysis in EGFR-mutated LAD cells. EGFR signaling regulates functional GLUT3 to control the glycolysis and pentose phosphate pathways. Moreover, EGFR signaling activated *de novo* pyrimidine synthesis, which is regulated by

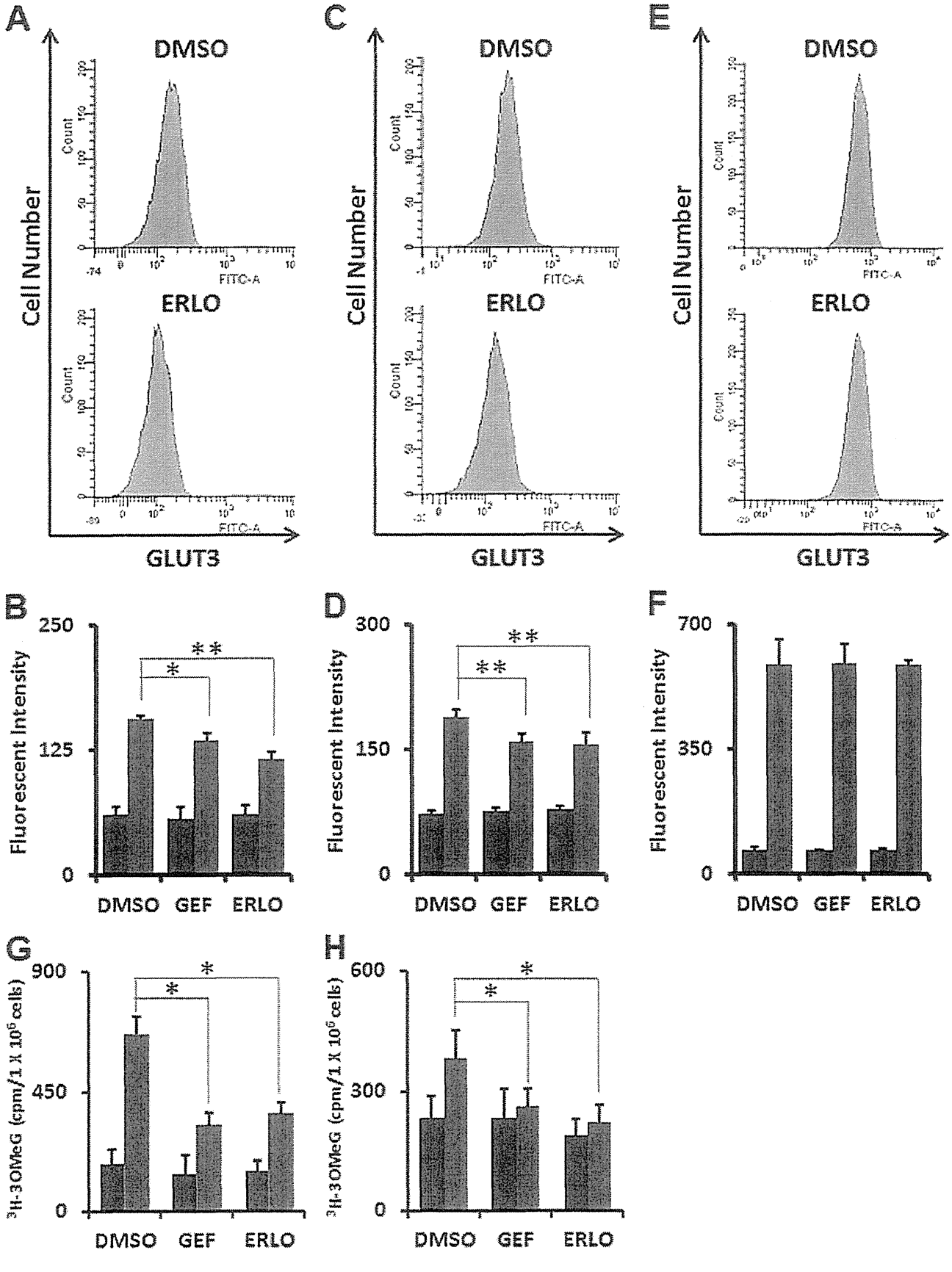

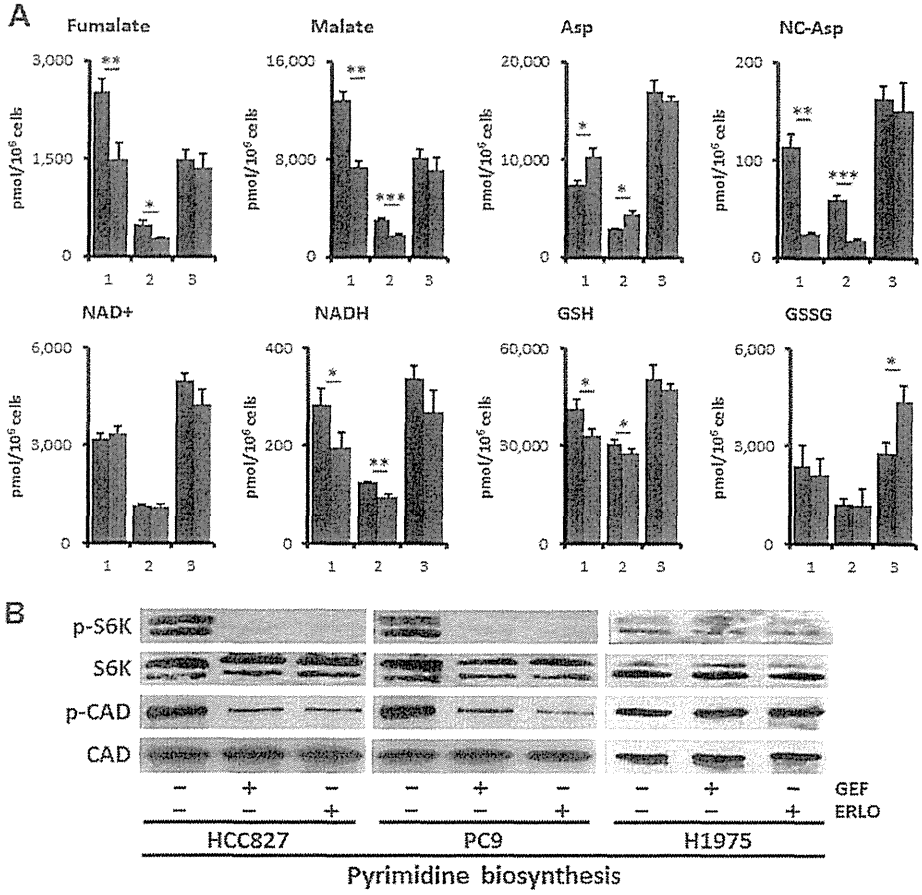

FIGURE 7. **EGFR signaling maintains *de novo* pyrimidine biosynthesis pathway.** *A*, metabolome analysis. Intracellular concentration (pmol/million cells) of key metabolites involved in glycolysis and pentose phosphate pathway (*PPP*) after inhibition of EGFR signaling is shown. Error bars indicate S.D. ($n = 3$). Total metabolites were extracted with methanol from HCC827, PC9, or H1975 cells treated with DMSO (*blue*) or erlotinib (*red*, 1 μM) for 6 h. Representative metabolites such as fumarate (*FA*), malate (*MA*), aspartate (*Asp*), *N*-carbamoyl-aspartate (NC-Asp), NAD^+, NADH, reductive glutathione (*GSH*), and oxidative glutathione (*GSSG*) are shown here. *B*, Western blot showing proteins related with *de novo* pyrimidine synthesis. Total protein lysates were isolated from cells treated with gefitinib (1 μM) or erlotinib (1 μM) for 6 h. Equivalent amounts of proteins from whole-cell lysates were subjected to Western blot analysis to detect the indicated proteins. Ribosomal protein S6 kinase 1 (S6K), phospho-S6K (p-S6K, Thr421/Ser424) and carbamoyl-phosphate synthetase 2, aspartate transcarbamoylase, dihydroorotase (CAD), and phospho-CAD (p-CAD, Ser-1859) are shown.

CAD activity. We conclude that EGFR signaling regulates global metabolic pathways in EGFR-mutated LAD cells. Our data provide evidence that may link the EGFR-TKI response to the regulation of metabolism in EGFR-mutated LAD. Inhibition of EGFR signaling abrogated the Warburg effect by inhibiting multiple steps including MYC-driven transcription and phosphorylation of PKM2 to regulate glycolysis in LAD. We comprehensively quantified the key metabolites in glycolysis and PPP and identified glucose transport as the most important regulatory step for controlling glucose metabolism in LAD cells during EGFR signaling. This observation is consistent with a previous study demonstrating that gefitinib treatment decreased glucose transport efficiency and hexokinase activity in TKI-sensitive LAD cells (26).

The molecular mechanism by which EGFR signaling regulates glucose transport is still unclear. Weihua *et al.* found that EGFR physically associated with and stabilized the sodium/glucose transporter (SGLT1) to promote glucose uptake into cancer

FIGURE 6. **Glucose transport efficiency is the most rapid and critically regulated function of glucose metabolism linked to EGFR signaling.** *A*, representative flow cytometry plot of GLUT3 expression in HCC827 cells treated with erlotinib (1 μM) or DMSO as a control for 6 h. After fixation, cells were stained with a rabbit anti-GLUT3 antibody and FITC-conjugated anti-rabbit secondary antibody. *B*, flow cytometric analysis of GLUT3 expression in HCC827 cells. *Blue bars* show background fluorescence with IgG isotype control while *red bars* indicate fluorescence staining results with anti-GLUT3 Ab. Error bars indicate S.D. ($n = 4$). *, $p < 0.05$; **, $p < 0.01$ *versus* control by two-tailed Student's *t* test. *C*, representative flow cytometry plot of GLUT3 expression in PC9 cells treated with erlotinib (1 μM) or DMSO as a control for 6 h. After fixation, cells were stained with a rabbit anti-GLUT3 antibody and FITC-conjugated anti-rabbit secondary antibody. *D*, flow cytometric analysis of GLUT1 expression in PC9 cells. *Blue bars* show background fluorescence with IgG isotype control while *red bars* indicate fluorescence staining results with anti-GLUT3 Ab. Error bars indicate S.D. ($n = 4$). *, $p < 0.05$; **, $p < 0.01$ *versus* control by two-tailed Student's *t* test. *E*, representative flow cytometry plot of GLUT3 expression in TKI-resistant H1975 cells treated with erlotinib (1 μM) or DMSO as a control for 6 h. After fixation, cells were stained with a rabbit anti-GLUT3 antibody and FITC-conjugated anti-rabbit secondary antibody. *F*, flow cytometric analysis of GLUT3 expression in TKI-resistant H1975 cells. *Blue bars* show background fluorescence with IgG isotype control while *red bars* indicate fluorescence staining results with anti-GLUT3 Ab. Error bars indicate S.D. ($n = 4$). *, $p < 0.05$; **, $p < 0.01$ *versus* control by two-tailed Student's *t* test. *G* and *H*, 3-*O*-([^{3}H]methyl)-D-glucose (3-OMeG) transport efficiency in HCC827 (*G*) and PC-9 (*H*) cells in response to gefitinib or erlotinib as compared with DMSO control. Cells were treated with indicated TKIs (1 μM) for 6 h before transport assay. Radioactivity was measured over time. Cells were harvested at 1 min (*blue*) and 10 min (*red*) after addition of 3-OMeG. Error bars indicate S.D. ($n = 4$). *, $p < 0.001$ *versus* control by two-tailed Student's *t* test.

cells (36). However, this function did not require EGFR kinase activity. In this report, we found that TKIs to EGFR, gefitinib, and erlotinib, repressed aerobic glycolysis and PPP in EGFR-mutated LAD cells. Although SGLT1 directly interacts with EGFR, EGFR signaling may regulate GLUT translocation in an indirect manner. Mutated EGFRs found in LAD have constitutive tyrosine kinase activity, resulting in activation of downstream RAS/MAPK and PI3K/AKT pathways (Figs. 4*A* and 5*B*). In adipocytes and skeletal muscle, insulin and the PI3K/AKT pathway mediate GLUT4 translocation (37, 38). To promote glucose uptake into muscle and fat cells, insulin stimulates the translocation of GLUT4 from intracellular membranes to the cell surface. Insulin signals go through AS160 (Akt substrate of 160 kDa) and Tbc1Ds to modulate Rab GTPase, and through Rho GTPase TC10a to act on other targets (37, 38). The EGFR-PI3K/AKT axis might control GLUT translocation to the plasma membrane in EGFR-mutated LAD cells. To prove this, we would need to characterize in more detail the molecular mechanisms that control GLUT expression, activity, and translocation.

A recent study showed that AMPK-dependent degradation of thioredoxin-interacting protein (TXNIP) upon stress led to enhanced glucose uptake via GLUT1 (39). Another research report showed that tumor-associated mutant p53 (mutp53) stimulated the Warburg effect in cancer cells as a new mutp53 gain of function (40). Mutp53 did not affect the expression of GLUT1, but promoted aerobic glycolysis by inducing GLUT1 translocation to the plasma membrane, which was mediated by activated RHOA and its downstream effector ROCK. In this study, the EGFR-TKI-sensitive LAD cell lines HCC827 and PC9 possess mutp53, but not the H1975 cell line. A possible molecular mechanism is that either EGFR signaling may regulate GLUT translocation by directly activating the RHOA/ROCK pathway or the mutp53 pathway that in turn activates RHOA/ROCK function. Further experiments would be required to determine whether EGFR signaling controls glucose transport through the TXNIP or mutp53 pathway.

New therapeutic strategies are currently needed to overcome the EGFR T790M-mediated acquired resistance observed in the clinic (8). A recent Phase III study of afatinib monotherapy failed to show overall survival benefit in patients with acquired resistance to reversible EGFR-TKIs(41). Kim *et al.* showed that targeting of glycolysis was an effective therapeutic option to overcome the limited efficacy of afatinib in LAD cells with EGFR T790M (42). Treatment with 2DG completely shut down lactate production in EGFR-mutated LAD cells (Fig. 2*B*), since 2DG is a glucose analog that competes with glucose for cellular uptake. Therefore, combination therapies of EGFR-TKIs and drugs that block the glycolysis pathway such as GLUT-inhibitors would be expected to be much more effective for TKI-resistant cases.

Molecular targeting therapy using TKIs is currently one of the most successful forms of treatment in the clinic, and includes imatinib targeting BCR-ABL in chronic myeloid leukemia (CML) and gefitinib/erlotinib in EGFR-mutated LAD (3). Despite high therapeutic responses to EGFR-TKI treatment, it is clear that not all patients experience benefit; thus, there is still a need to identify potential non-responders and match patients with the most effective therapies (4). Monitoring of tumor glucose utilization by [^{18}F]fluorodeoxyglucose (FDG)-positron emission tomography (PET) was implemented for the early prediction of treatment response to EGFR-TKIs in NSCLC (26, 43). In this report, we demonstrate that TKIs to EGFR, gefitinib and erlotinib, repress aerobic glycolysis in EGFR-mutated LAD cells. Those correlations strongly suggest that intermediate metabolites in the pentose phosphate pathway, glycolysis, and pyrimidine biosynthesis such as FBP, DHAP, LA, 6PG, and NC-Asp could serve as well-defined biomarkers to predict response to EGFR-TKI therapy.

The application of metabolomics in oncology has focused its ability to identify biomarkers for cancer diagnosis, prognosis, and therapeutic efficacy (44). In our previous study, we compared the metabolomics of normal and tumor tissues surgically resected pairwise from nine lung patients using CE-TOFMS to elucidate tumor-specific metabolism (45). Significantly high lactate concentrations and elevated activating phosphorylation levels of phosphofructokinase and pyruvate kinase in lung tumors confirmed hyperactive glycolysis (45). Here we show that EGFR signaling regulates many metabolites in EGFR-mutated LAD cells under *in vitro* culture conditions; however, whether EGFR-TKIs have the same effects *in vivo* is still unknown. To build upon this work, further investigations will explore these concepts in relevant animal models and in LAD tissue biopsy samples using bronchoscope before and after EGFR-TKI therapy. *In vivo* validation of these concepts will have significant implications for future diagnostic and therapeutic possibilities for patients.

Acknowledgments—We thank all of Dr. Tsuchihara's laboratory members for help. We also thank Dr. Phillip Wong for carefully reading the manuscript and providing critical comments.

REFERENCES

1. da Cunha Santos, G., Shepherd, F. A., and Tsao, M. S. (2011) EGFR mutations and lung cancer. *Annu. Rev. Pathol.* **6,** 49–69
2. Irmer, D., Funk, J. O., and Blaukat, A. (2007) EGFR kinase domain mutations - functional impact and relevance for lung cancer therapy. *Oncogene* **26,** 5693–5701
3. Levitzki, A. (2013) Tyrosine kinase inhibitors: views of selectivity, sensitivity, and clinical performance. *Annu. Rev. Pharmacol. Toxicol.* **53,** 161–185
4. Linardou, H., Dahabreh, I. J., Bafaloukos, D., Kosmidis, P., and Murray, S. (2009) Somatic EGFR mutations and efficacy of tyrosine kinase inhibitors in NSCLC. *Nat. Rev. Clin. Oncol.* **6,** 352–366
5. Suzuki, A., Mimaki, S., Yamane, Y., Kawase, A., Matsushima, K., Suzuki, M., Goto, K., Sugano, S., Esumi, H., Suzuki, Y., and Tsuchihara, K. (2013) Identification and characterization of cancer mutations in Japanese lung adenocarcinoma without sequencing of normal tissue counterparts. *PLoS One* **8,** e73484
6. Imielinski, M., Berger, A. H., Hammerman, P. S., Hernandez, B., Pugh, T. J., Hodis, E., Cho, J., Suh, J., Capelletti, M., Sivachenko, A., Sougnez, C., Auclair, D., Lawrence, M. S., Stojanov, P., Cibulskis, K., Choi, K., de Waal, L., Sharifnia, T., Brooks, A., Greulich, H., Banerji, S., Zander, T., Seidel, D., Leenders, F., Ansén, S., Ludwig, C., Engel-Riedel, W., Stoelben, E., Wolf, J., Goparju, C., Thompson, K., Winckler, W., Kwiatkowski, D., Johnson, B. E., Jänne, P. A., Miller, V. A., Pao, W., Travis, W. D., Pass, H. I., Gabriel, S. B., Lander, E. S., Thomas, R. K., Garraway, L. A., Getz, G., and Meyerson, M. (2012) Mapping the Hallmarks of Lung Adenocarcinoma with Massively Parallel Sequencing. *Cell* **150,** 1107–1120
7. Mellinghoff, I. (2007) Why do cancer cells become "addicted" to oncogenic epidermal growth factor receptor? *Plos Med.* **4,** 1620–1622

8. Pao, W., and Chmielecki, J. (2010) Rational, biologically based treatment of EGFR-mutant non-small-cell lung cancer. *Nature Reviews Cancer* **10,** 760–774
9. Lemmon, M. A., and Schlessinger, J. (2010) Cell signaling by receptor tyrosine kinases. *Cell* **141,** 1117–1134
10. Cairns, R. A., Harris, I. S., and Mak, T. W. (2011) Regulation of cancer cell metabolism. *Nat. Rev. Cancer* **11,** 85–95
11. Levine, A. J., and Puzio-Kuter, A. M. (2010) The control of the metabolic switch in cancers by oncogenes and tumor suppressor genes. *Science* **330,** 1340–1344
12. Cheong, H., Lu, C., Lindsten, T., and Thompson, C. B. (2012) Therapeutic targets in cancer cell metabolism and autophagy. *Nat. Biotechnol.* **30,** 671–678
13. Ying, H., Kimmelman, A. C., Lyssiotis, C. A., Hua, S., Chu, G. C., Fletcher-Sananikone, E., Locasale, J. W., Son, J., Zhang, H., Coloff, J. L., Yan, H., Wang, W., Chen, S., Viale, A., Zheng, H., Paik, J. H., Lim, C., Guimaraes, A. R., Martin, E. S., Chang, J., Hezel, A. F., Perry, S. R., Hu, J., Gan, B., Xiao, Y., Asara, J. M., Weissleder, R., Wang, Y. A., Chin, L., Cantley, L. C., and DePinho, R. A. (2012) Oncogenic Kras maintains pancreatic tumors through regulation of anabolic glucose metabolism. *Cell* **149,** 656–670
14. Lunt, S. Y., and Vander Heiden, M. G. (2011) Aerobic glycolysis: meeting the metabolic requirements of cell proliferation. *Annu. Rev. Cell Dev. Biol.* **27,** 441–464
15. Soga, T. (2013) Cancer metabolism: key players in metabolic reprogramming. *Cancer Sci.* **104,** 275–281
16. Vander Heiden, M. G., Cantley, L. C., and Thompson, C. B. (2009) Understanding the Warburg effect: the metabolic requirements of cell proliferation. *Science* **324,** 1029–1033
17. Hitosugi, T., Kang, S., Vander Heiden, M. G., Chung, T. W., Elf, S., Lythgoe, K., Dong, S., Lonial, S., Wang, X., Chen, G. Z., Xie, J., Gu, T. L., Polakiewicz, R. D., Roesel, J. L., Boggon, T. J., Khuri, F. R., Gilliland, D. G., Cantley, L. C., Kaufman, J., and Chen, J. (2009) Tyrosine phosphorylation inhibits PKM2 to promote the Warburg effect and tumor growth. *Sci. Signal* **2,** ra73
18. Hitosugi, T., and Chen, J. (2013) Post-translational modifications and the Warburg effect. *Oncogene* doi:10.1038/onc.2013.406
19. Miller, D. M., Thomas, S. D., Islam, A., Muench, D., and Sedoris, K. (2012) c-Myc and cancer metabolism. *Clin. Cancer Res.* **18,** 5546–5553
20. Yang, W., and Lu, Z. (2013) Nuclear PKM2 regulates the Warburg effect. *Cell Cycle* **12,** 3154–3158
21. Wong, N., Ojo, D., Yan, J., and Tang, D. (2014) PKM2 contributes to cancer metabolism. *Cancer Lett.* doi: 10.1016/j.canlet. 2014.01.031
22. Babic, I., Anderson, E. S., Tanaka, K., Guo, D., Masui, K., Li, B., Zhu, S., Gu, Y., Villa, G. R., Akhavan, D., Nathanson, D., Gini, B., Mareninov, S., Li, R., Camacho, C. E., Kurdistani, S. K., Eskin, A., Nelson, S. F., Yong, W. H., Cavenee, W. K., Cloughesy, T. F., Christofk, H. R., Black, D. L., and Mischel, P. S. (2013) EGFR mutation-induced alternative splicing of Max contributes to growth of glycolytic tumors in brain cancer. *Cell Metab.* **17,** 1000–1008
23. Soga, T., and Heiger, D. N. (2000) Amino acid analysis by capillary electrophoresis electrospray ionization mass spectrometry. *Anal. Chem.* **72,** 1236–1241
24. Soga, T., Ueno, Y., Naraoka, H., Ohashi, Y., Tomita, M., and Nishioka, T. (2002) Simultaneous determination of anionic intermediates for Bacillus subtilis metabolic pathways by capillary electrophoresis electrospray ionization mass spectrometry. *Anal. Chem.* **74,** 2233–2239
25. Soga, T., Ohashi, Y., Ueno, Y., Naraoka, H., Tomita, M., and Nishioka, T. (2003) Quantitative metabolome analysis using capillary electrophoresis mass spectrometry. *J. Proteome Res.* **2,** 488–494
26. Su, H., Bodenstein, C., Dumont, R. A., Seimbille, Y., Dubinett, S., Phelps, M. E., Herschman, H., Czernin, J., and Weber, W. (2006) Monitoring tumor glucose utilization by positron emission tomography for the prediction of treatment response to epidermal growth factor receptor kinase inhibitors. *Clin. Cancer Res.* **12,** 5659–5667
27. Okamoto, K., Okamoto, I., Okamoto, W., Tanaka, K., Takezawa, K., Kuwata, K., Yamaguchi, H., Nishio, K., and Nakagawa, K. (2010) Role of survivin in EGFR inhibitor-induced apoptosis in non-small cell lung cancers positive for EGFR mutations. *Cancer Res.* **70,** 10402–10410
28. Donev, I. S., Wang, W., Yamada, T., Li, Q., Takeuchi, S., Matsumoto, K., Yamori, T., Nishioka, Y., Sone, S., and Yano, S. (2011) Transient PI3K inhibition induces apoptosis and overcomes HGF-mediated resistance to EGFR-TKIs in EGFR mutant lung cancer. *Clin. Cancer Res.* **17,** 2260–2269
29. Zhou, W., Ercan, D., Chen, L., Yun, C. H., Li, D., Capelletti, M., Cortot, A. B., Chirieac, L., Iacob, R. E., Padera, R., Engen, J. R., Wong, K. K., Eck, M. J., Gray, N. S., and Jänne, P. A. (2009) Novel mutant-selective EGFR kinase inhibitors against EGFR T790M. *Nature* **462,** 1070–1074
30. Sudo, M., Chin, T. M., Mori, S., Doan, N. B., Said, J. W., Akashi, M., and Koeffler, H. P. (2013) Inhibiting proliferation of gefitinib-resistant, non-small cell lung cancer. *Cancer Chemother. Pharmacol.* **71,** 1325–1334
31. Sonveaux, P., Végran, F., Schroeder, T., Wergin, M. C., Verrax, J., Rabbani, Z. N., De Saedeleer, C. J., Kennedy, K. M., Diepart, C., Jordan, B. F., Kelley, M. J., Gallez, B., Wahl, M. L., Feron, O., and Dewhirst, M. W. (2008) Targeting lactate-fueled respiration selectively kills hypoxic tumor cells in mice. *J. Clin. Invest.* **118,** 3930–3942
32. Morrish, F., Neretti, N., Sedivy, J. M., and Hockenbery, D. M. (2008) The oncogene c-Myc coordinates regulation of metabolic networks to enable rapid cell cycle entry. *Cell Cycle* **7,** 1054–1066
33. Osthus, R. C., Shim, H., Kim, S., Li, Q., Reddy, R., Mukherjee, M., Xu, Y., Wonsey, D., Lee, L. A., and Dang, C. V. (2000) Deregulation of glucose transporter 1 and glycolytic gene expression by c-Myc. *J. Biol. Chem.* **275,** 21797–21800
34. David, C. J., Chen, M., Assanah, M., Canoll, P., and Manley, J. L. (2010) HnRNP proteins controlled by c-Myc deregulate pyruvate kinase mRNA splicing in cancer. *Nature* **463,** 364–368
35. Ben-Sahra, I., Howell, J. J., Asara, J. M., and Manning, B. D. (2013) Stimulation of de novo pyrimidine synthesis by growth signaling through mTOR and S6K1. *Science* **339,** 1323–1328
36. Weihua, Z., Tsan, R., Huang, W. C., Wu, Q., Chiu, C. H., Fidler, I. J., and Hung, M. C. (2008) Survival of cancer cells is maintained by EGFR independent of its kinase activity. *Cancer Cell* **13,** 385–393
37. Watson, R. T., and Pessin, J. E. (2006) Bridging the GAP between insulin signaling and GLUT4 translocation. *Trends Biochem. Sci.* **31,** 215–222
38. Bogan, J. S. (2012) Regulation of glucose transporter translocation in health and diabetes. *Annu. Rev. Biochem.* **81,** 507–532
39. Wu, N., Zheng, B., Shaywitz, A., Dagon, Y., Tower, C., Bellinger, G., Shen, C. H., Wen, J., Asara, J., McGraw, T. E., Kahn, B. B., and Cantley, L. C. (2013) AMPK-dependent degradation of TXNIP upon energy stress leads to enhanced glucose uptake via GLUT1. *Mol. Cell* **49,** 1167–1175
40. Zhang, C., Liu, J., Liang, Y., Wu, R., Zhao, Y., Hong, X., Lin, M., Yu, H., Liu, L., Levine, A. J., Hu, W., and Feng, Z. (2013) Tumour-associated mutant p53 drives the Warburg effect. *Nat. Commun.* **4,** 2935
41. Miller, V. A., Hirsh, V., Cadranel, J., Chen, Y. M., Park, K., Kim, S. W., Zhou, C., Su, W. C., Wang, M., Sun, Y., Heo, D. S., Crino, L., Tan, E. H., Chao, T. Y., Shahidi, M., Cong, X. J., Lorence, R. M., and Yang, J. C. (2012) Afatinib versus placebo for patients with advanced, metastatic non-small-cell lung cancer after failure of erlotinib, gefitinib, or both, and one or two lines of chemotherapy (LUX-Lung 1): a phase 2b/3 randomised trial. *Lancet Oncol.* **13,** 528–538
42. Kim, S. M., Yun, M. R., Hong, Y. K., Solca, F., Kim, J. H., Kim, H. J., and Cho, B. C. (2013) Glycolysis inhibition sensitizes non-small cell lung cancer with T790M mutation to irreversible EGFR inhibitors via translational suppression of Mcl-1 by AMPK activation. *Mol. Cancer Ther.* **12,** 2145–2156
43. Takahashi, R., Hirata, H., Tachibana, I., Shimosegawa, E., Inoue, A., Nagatomo, I., Takeda, Y., Kida, H., Goya, S., Kijima, T., Yoshida, M., Kumagai, T., Kumanogoh, A., Okumura, M., Hatazawa, J., and Kawase, I. (2012) Early [18F]fluorodeoxyglucose positron emission tomography at two days of gefitinib treatment predicts clinical outcome in patients with adenocarcinoma of the lung. *Clin. Cancer Res.* **18,** 220–228
44. Spratlin, J. L., Serkova, N. J., and Eckhardt, S. G. (2009) Clinical applications of metabolomics in oncology: a review. *Clin. Cancer Res.* **15,** 431–440
45. Kami, K., Fujimori, T., Sato, H., Sato, M., Yamamoto, H., Ohashi, Y., Sugiyama, N., Ishihama, Y., Onozuka, H., Ochiai, A., Esumi, H., Soga, T., and Tomita, M. (2013) Metabolomic profiling of lung and prostate tumor tissues by capillary electrophoresis time-of-flight mass spectrometry. *Metabolomics* **9,** 444–453

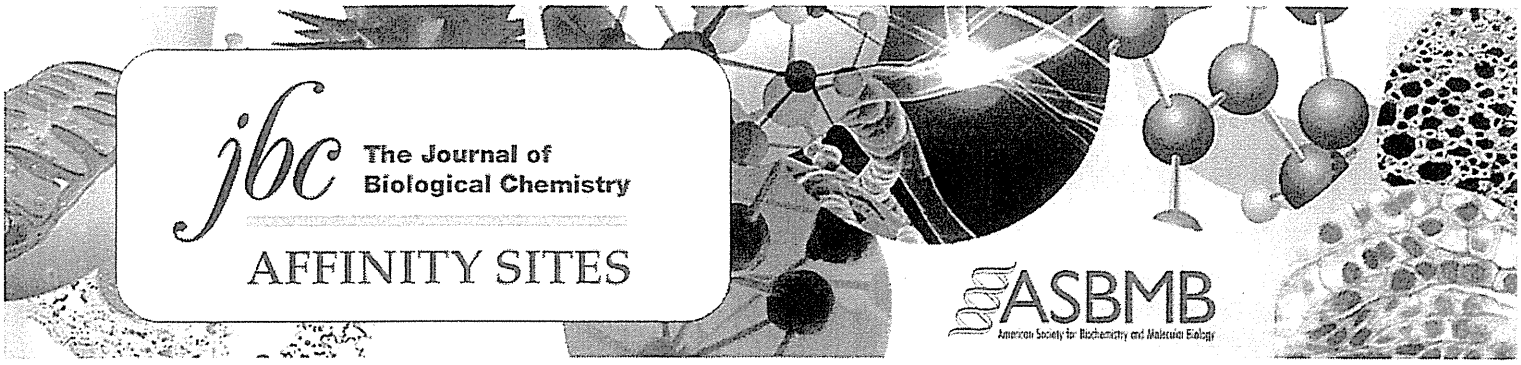

Metabolism:

Epidermal Growth Factor Receptor (EGFR) Signaling Regulates Global Metabolic Pathways in EGFR-mutated Lung Adenocarcinoma

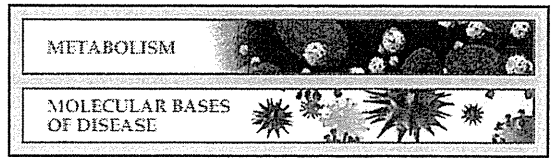

Hideki Makinoshima, Masahiro Takita, Shingo Matsumoto, Atsushi Yagishita, Satoshi Owada, Hiroyasu Esumi and Katsuya Tsuchihara

J. Biol. Chem. 2014, 289:20813-20823.
doi: 10.1074/jbc.M114.575464 originally published online June 13, 2014
